Master's Thesis
석사 학위논문

Structural and Electrochemical Characterizations of FeV_3O_8 as a Host Material for Rechargeable Li - ion Batteries

Sang-Hun Lee (이 상 훈 李 尙 勳)

Department of Energy Systems Engineering
에너지시스템공학전공

DGIST

2016

Master's Thesis
석사 학위논문

Structural and Electrochemical Characterizations of FeV_3O_8 as a Host Material for Rechargeable Li - ion Batteries

Sang-Hun Lee(이 상 훈 李 尙 勳)

Department of Energy Systems Engineering
에너지시스템공학전공

DGIST

2016

Structural and Electrochemical Characterizations of FeV_3O_8 as a Host Material for Rechargeable Li - ion Batteries

Advisor : Professor Seung-Tae Hong

Co-advisor : Doctor Jae-Hyun Kim

by

Sang-Hun Lee

Department of Energy Systems Engineering

DGIST

A thesis submitted to the faculty of DGIST in partial fulfillment of the requirements for the degree of Master of Science in the Department of Energy Systems Engineering. The study was conducted in accordance with Code of Research Ethics[1]

12. 01. 2015

Approved by

Professor (Advisor) Seung-Tae Hong (Signature)

Doctor Jae-Hyun Kim (Signature)

[1] Declaration of Ethical Conduct in Research: I, as a graduate student of DGIST, hereby declare that I have not committed any acts that may damage the credibility of my research. These include, but are not limited to: falsification, thesis written by someone else, distortion of research findings or plagiarism. I affirm that my thesis contains honest conclusions based on my own careful research under the guidance of my thesis advisor.

Structural and Electrochemical Characterizations of FeV_3O_8 as a Host Material for Rechargeable Li - ion Batteries

Sang-Hun Lee

Accepted in partial fulfillment of the requirements for the degree of Master of Science.

12. 01. 2015

Head of Committee Seung-Tae Hong (인)

Prof. Seung-Tae Hong

Committee Member 이 호 춘 (인)

Prof. Hochun Lee

Committee Member 김 재 현 (인)

Dr. Jae-Hyun Kim

MS/ES

201324009

이 상 훈. Sang-Hun Lee. Structural and Electrochemical Characterizations of FeV_3O_8 as a Host Material for Rechargeable Li - ion Batteries
Department of Energy Systems Engineering.

2016. 47p. Advisors Prof. Seung-Tae Hong. Co-Advisors Dr. Jae-Hyun Kim.

Abstract

We investigate how affected by intercalation chemistry of lithium ion into monoclinic FeV_3O_8 tunnel structure. By using high temperature solid state synthetic method, rod-type FeV_3O_8 powder could be obtained and then, confirm powder phase and morphology by using SEM and XRD.

In order to determine lithium ion intercalation profiles into those structure, several structural and electrochemical features such as cyclic voltammetry, galvanostatic discharge/charge curve and XRD analysis were conducted. Although FeV_3O_8 as a positive electrode would be operated with unfavorable performance that could not be utilized to satisfy performances of EV needs given period of time, we discovered possibility of these material through structural and electrochemical studies during project.

As a novel positive material, FeV_3O_8 vs. Lithium cell discharged at 0.2C (1C = 151.9mAh g^{-1}) delivered 63.51mAh/g of reversible capacity with the electrochemically active redox reaction. In the voltage range between 2.0 – 3.5V, the cell exhibits one voltage plateaus with well- defined discharge voltage near 2.7 V, and a coulombic efficiency of approximately 99 percent. Unfortunately, FeV_3O_8 has poor high-rate performances, the cell exhibits a specific capacity of about 5 mAh g^{-1} at 10C. These results are caused to the crystallized particle morphology.

We have been investigating several countermeasures for contributing lithium ion intercalation into FeV_3O_8 structure. In order to improve kinetic properties, the change of particle size and morphology to submicron size has to be considered. As an other example, additional coating process onto particles surface using high conductivity materials could be increased profiles of kinetic into the host materials.

Keyword: monoclinic FeV_3O_8, Tunnel-like structure, 1-D diffusion path, positive electrode

List of Contents

List of Figures

List of Tables

1. Introduction

The energy resources such as fossil fuels are necessary to our lives. These days, however, the fossil fuels are at a severe risk because of demand for oil that increase continuously, lack of limited energy sources, and complicated political situation of fossil fuel production countries. Moreover, the fossil fuels emit CO_2 gas during combustion caused by global climate problems.

To solve this problem, the renewable energy resources such as solar power, wind power and etc. have been received attention to many researchers in the various fields. Recently, rechargeable batteries for energy storage systems have emerged as the significant area for portable power sources in the modern society. [1] Moreover, an effective high-capacity secondary battery is required as a key component of electrical vehicles and high-capacity stationary electricity storage systems. Among the various secondary batteries available, rechargeable Li-ion cells are a good candidate for such purposes (the portable, entertainment, computing and hybrid & EV) due to its high capacity and well-developed infrastructure.[1]

Future power hybrid vehicles and electric vehicles (EV) area are needed to large energy density (500Wh/kg) to be competitive in driving range and cost to vehicles powered by combustion engines.[2] Lithium-based rechargeable batteries are, however, being almost reached theoretical energy density (300Wh/kg) that is insufficient requirements for EV system. In addition, the sources of lithium have limited to specific area as poorly accessible forms, *e.g.* 0.04-1.16% in brine ponds, which require about 1 year for the final production of lithium carbonate.[3] Moreover, lithium-based metal is not environmentally friendly, safe and therefore, there is a need for high recycling costs or proper disposal to prevent dissemination of the toxic elements into the environment.

As a result, the new concept of components that form the positive and negative electrodes for rechargeable Li - ion cells in electrical power applications of the future have to be essentially developed due to their various technical issues and cost barriers as well as the inherent safety and growing environmental concern. [1–3] Therefore, rechargeable Li-ion batteries have still the object of intense research with the aim of further increasing their properties and characteristics.

1.1 The principle of lithium based rechargeable batteries

The motivation for using a battery technology based on Li metal as anode referred to the fact that Li has the low electropositive voltage (–3.04 V vs. standard hydrogen electrode) as well as the lightest metal, thus implementing the design of storage systems with high energy density. The benefits in using Li metal were demonstrated in the 1970s with primary-Li cells (not rechargeable). Owing to their high performance, primary Li cells rapidly utilized various industrial field as power sources for watches, calculators. In the same period, enormous inorganic compounds were reported to react with alkali metals in a reversible reaction.[2] The discovery of such materials, which were later investigated as intercalation compounds, was significant in the development of high-energy rechargeable Li - cell systems. By 1972, the concept of electrochemical intercalation and its potential use were clearly defined[4], although the information was not widely disseminated and being reported only in conference presentations.

Exxon[1] was reported to new concept of rechargeable Li cells using TiS_2 as the positive electrode, Li metal as the negative electrode and lithium perchlorate in dioxolane as the electrolyte in 1972. This report suggested TiS_2 is the best intercalation compound available at the time, having a layered-type structure.[5–8] In spite of the immaculate operation of the positive electrode, TiS_2 could not be commercialized for secondary battery. Other workers encountered the critical problem with a Li-metal/liquid electrolyte combination - dendrite formation onto Li-metal/liquid interface during each subsequent discharge/charge cycle (Fig. 2a)[1], which change to hazardous things with burst. Replacing Li metal for an alloy with Al solved the dendrite problem is a main key factor. This is because alloy electrodes between Li metal and Al survived only a limited number of cycles due to drastic volume changes during operation. In the meanwhile, Bell Labs investigated significant advances in intercalation oxide material for using the heavier chalcogenides which can be operated with higher capacities and voltages.

In early 1990s, improved and environmental friendly Ni-Mn batteries were commercialized. After 1990s, commercialized rechargeable batteries have to consist of four parts such as positive electrode and negative electrode that have structure facilitating intercalation with carrier ion, electrolyte and separator.

At the same time, emergence of lithium rechargeable batteries has been contributed portable devices market, such as mobile phone, laptop PC and etc. by improving energy density facilitating weight lightening[2]. Fig 1. indicates performance for operation with various species of rechargeable battery.[1]

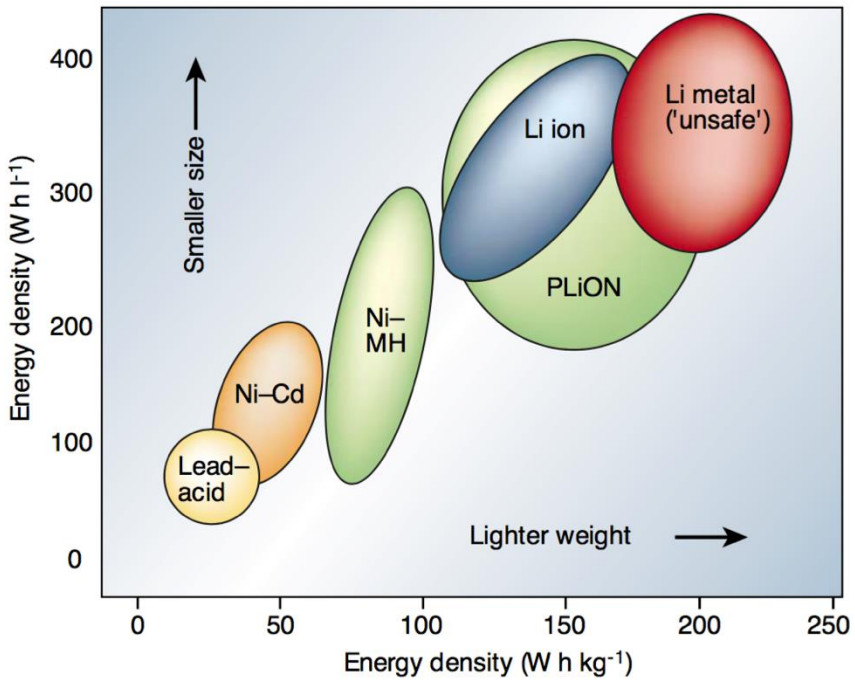

Figure 1. Comparison of the different battery technologies in terms of volumetric and gravimetric energy density[1]

Fundamentally, a rechargeable battery is an energy storage device and its principle is controlled the free energy correlation between a chemical reaction and electrochemical reaction is such that it can be stored for extended periods of time. A battery converts this chemical energy (energy related with bonds within the electrode material) into electrical energy (a characteristic electrical potential which can set electrons behavior). Ultimately, electrode materials and species of carrier ions would be the important factor to determine storage capability of electric energy. Batteries are generally categorized as primary (one time use-energy generation devices) or secondary (reversible use-energy storage devices). When the battery use lithium ions (Li+) as carrier ion with reversible redox reaction, the battery is called as lithium secondary battery (Figure. 2b). Main reaction into battery can be classified two parts such conversion reaction (e.g. lead acid) or intercalation reaction (e.g. lithium ion)[9].

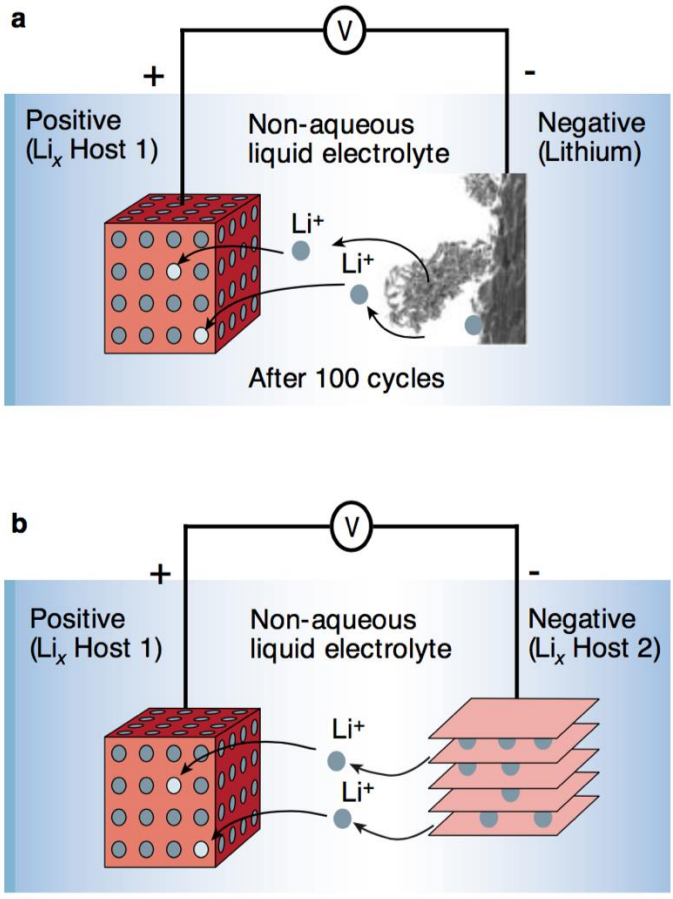

Figure 2. Schematic representation and operating principles of Li batteries. a) Rechargeable Li metal battery b) Rechargeable Li-ion battery[1]

Lithium ion rechargeable batteries have to use organic based electrolyte in order to have high operation voltage over water decomposition voltage, and materials having lattice structure that is easy to insertion and extraction for electrodes[10]. We focused on research direction to development of positive electrode and next section is referred to various species of positive electrode and explain of FeV_3O_8 material which has a monoclinic structure.

1.2 The cathode candidates for Li based battery system

1.2.1 Literature survey

It is generally used in a lithium ion battery using the negative electrode a carbon material and a compound containing lithium in the positive electrode. In the middle of 1970s, layer compounds, TiS_2, to insertion and desorption of lithium by electrochemical intercalation had been proposed that a lithium ion battery positive electrode by Whittingham.[9] In the early 1980's, the US Goodenough's group has proposed that the new cathode $LiCoO_2$ which is the α-$NaFeO_2$ layer structure material showing a charge-discharge potential of more than 4 V (vs. Li / Li^+).[4,11] In recent years, the most positive electrode active material is $LiCoO_2$ and then many researchers are looking for other oxide material using other transition metals than Co to replace the market of layered structure positive materials. In order to be next generation cathodes, the requirements of the active cathode material of lithium are having high discharge voltage, high capacity, high power, long life cycle, safety, economics and etc.

$LiCoO_2$

Typical cathode material of $LiCoO_2$ for lithium secondary battery was introduced for the first time by the Goodenough's group. In 1991, $LiCoO_2$ received much attention due to the successful commercialization of the rechargeable Li-ion battery and then a lot of research has still been researching $LiCoO_2$-base materials for improvements. $LiCoO_2$ which has a layer of α-$NaFeO_2$ structure (s.g. R-3m) is a consisting of CoO_2 and Li layer in CCP-packed (Co^{3+} : 3a site, Li^+ : 3b site). The theoretical capacity of $LiCoO_2$ is 274$mAhg^{-1}$ when all the lithium ion. In practice, however, only the lithium-ion of about half could be operated with the reversible intercalation / de-intercalation (≤ 4.2 V vs. Li / Li^+).[4,11,12]

$LiMn_2O_4$

One of the popular positive electrode material could be applied to the electric car is a spinel $LiMn_2O_4$. This material is used to $Mn^{3+/4+}$ in the oxidation/reduction process, which has a chemical stability of the cell. Because of chemical stability, $LiMn_2O_4$ have excellent power characteristics in a three-dimensional structure. In addition, Mn has a low price and also has eco-friendly benefits. Operating voltage is 4.1 V or $LiMn_2O_4$, a substituted form of the spinel group such as Li $[Ni_{0.5}Mn_{1.5}]O_4$ spinel structure material for high voltage as the operating voltage is 4.7 V is also receiving a lot of attention. In $LiMn_2O_4$ lithium has a cubic-closed packed O^{2-} position is located in the tetrahedral lattice of 8d site and Mn^{3+} 16c site of the octahedron. Spinel has been a lot of research is in progress to date in the 1990s, with the hetero atoms is substituted with $LiMn_2O_4$ material greatly improved electrical chemical performance.[11,13]

$LiFePO_4$

Representative cathode material is a olivine $LiFePO_4$. Iron as one of the most abundant metal is low cost than Co is environmentally friendly. Although Fe^{3+} / Fe^{2+} have an operating voltage about 3.2V (vs. Li / Li^+), $LiFePO_4$ is possible to obtain 3.4V (vs. Li / Li^+) due to the effect caused by a strong covalent bond of P-O and acid anion PO_4^{3-}. In addition, the advantage of the strong covalent bonds lead to structural stability at high temperature. Theoretical density of $LiFePO_4$ is 3.6 g cm^{-3} relatively low compared to other positive electrode materials and a theoretical capacity of 170 mAh g^{-1}.[10,14]

One of the biggest problems of $LiFePO_4$ shows a low electrical conductivity. This is a general characteristic of the material including multi-acid anions such as PO_4^{3-}. During charge/discharge, $LiFePO_4$ not only would be occurred severe polarization effect but also could be happened falling discharge capacity dramatically having uniformity of conductive material.

1.2.2 Tunnel structure, monoclinic FeV_3O_8

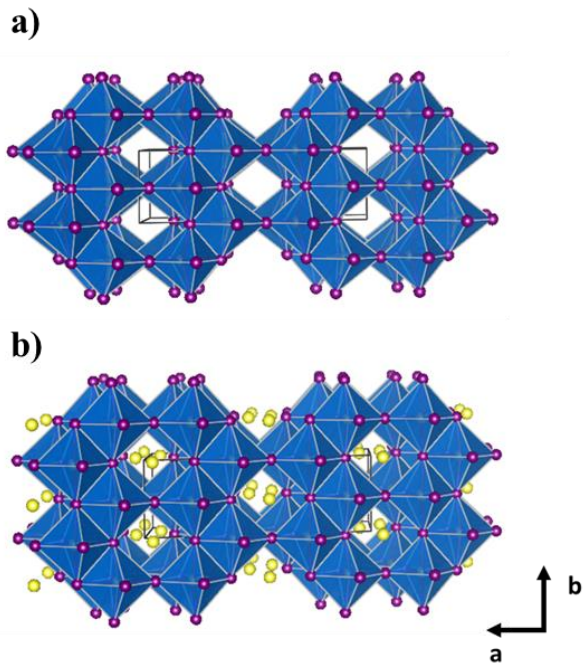

Figure 3 A schematic crystal structure of monoclinic a) FeV_3O_8 and b) $Li_2FeV_3O_8$

The crystal lattice expected for a (2x2) shear structure of the ReO3 lattice[15] is exhibited by the structures of VO_2 (B), TiO_2 (B), $AlNbO_4$ and FeV_3O_8.[15–21] Among these materials, we investigated the Li-ion cell characterization for Li-ion intercalation reaction with FeV_3O_8 electrode materials. Figure 3 presents a view of the crystal structure down the monoclinic c axis. It can be showed framework as a tunnel structure is consisted of the ReO_3 type polyhedral and edge sharing of the VO_2 (B) type structure.[22,16]

The mixed metal compound FeV_3O_8 was reported by Muller, et al, [16] from a molten vanadium oxide flux indicating thermal stability.

Y. HOTTA and S. KACHI investigated much work done on the $Fe_xV_{1-x}O_2$ ($0 \leq x \leq 0.5$) system according to the purpose of inorganic material synthetic study.[21] At the same time, they have been interested in materials which can move reversible intercalation of lithium ion for using as a cathode in rechargeable batteries. In order to utilize the fields of rechargeable batteries, we investigate whether be utilized electrode material for Li-ion battery as a cathode or not at the first time. First of all, we carried out designing synthesis conditions of FeV_3O_8 and conducted with electrochemical characterizations with Li-ion. The detail process has shown other sections.

Furthermore, to understand the complex mechanism of lithium ion electrochemical intercalation into FeV_3O_8 structure, we have been extending the sight of structural aspect with crystallography how structure changed during intercalation/de-intercalation process.

2. Experiments

2.1 Preparation of sample

Tunnel structure FeV_3O_8 compound was synthesized by using high temperature solid state synthetic method. Stoichiometric amounts of Fe_2O_3 (Aldrich, 99%), V_2O_5 (Alfa, 99.6%), and V_2O_3 (reduction reaction from V_2O_5 – Alfa, 99.6%) with molar ratio 1 : 2 : 1 were used as starting materials. One report was introduced by Morin research on the impurity effect of the phase transition of VO_2 in $Fe_xV_{1-x}O_2$ ($0 \leq x \leq 0.5$)[21]. In order to make a FeV_3O_8 structure without any secondary phase such as VO_2, stoichiometric ratios of starting materials were modified (modified composition : $Fe_{1.1}V_{2.9}O_8$). The precursor mixture was pressed into a pellet, heated for 36 hours at 800℃ (increase rate : 1.3℃/min) in a vacuum-sealed fused-silica tube, and then quenched in cool water.

2.2 The material characterization

XRD

The crystallographic structure of the as prepared material was studied by using XRD on a Miniflex 600 Rigaku with mono-chromatic CuKα radiation (λ=1.5418 Å), and the powder X-ray diffraction data were recorded in the angular range of $20° \leq 2\theta \leq 80°$ with a step size of 0.02° and a duration time of 5s for a general purpose. Crystal structures for FeV_3O_8 was refined using the powder profile refinement program GSAS.

Scanning Electron Microscope (SEM)

The particle morphology of the composite was investigated by using S-4800, HITACHI scanning electron microscope.

2.3 Preparation of electrodes and electrolyte

The electrochemical characterizations were determined with CR 2032 coin cells which contained FeV3O8 and lithium metal anode separated by porous polypropylene. The galvanostatic discharge/charge performances of the synthesized samples were conducted on channels battery analyzer (Toyo) at different current densities between 2.0 and 3.5 V. The cyclic voltammetry measurements were conducted on VMP-3 (EC-LAB) electrochemical workstation. The voltage range of the cyclic voltammetry measurements was 2.0 - 3.5V and the scanning rate was 0.1mV s^{-1}. All electrochemical tests were conducted at room temperature.

Working electrode

FeV_3O_8 electrode was fabricated via a traditional pressed powder film method. Electrodes slurry were made of active material (FeV_3O_8), acetylene black, and binder (Polyvinyli-dene fluoride, PvdF) in a weight ratio of 8 : 1 : 1 dissolved in N-methyl-2-pyrrolidone using a Thinky mixer (Thinky). The slurry was coated onto 15um thick aluminum (Al) foil using a doctor blade and mini-coater (Hohsen). The coated electrodes pressed to a film thickness of 50um via a roller press (Wellcos Corporation) and then, were dried under vacuum at 120℃ for 24h and stored in an argon (Ar) filled glove box. The electrodes have a loading density of ~0.31mAh/cm^2, and porosity of ~73%.

Counter electrode

Li metal as an anode

Electrolyte

1M $LiPF_6$ in EC/DMC (1 : 2 by volume)

3. Results and Discussion

3.1 Material characterizations

In order to prepare the FeV_3O_8 powders, synthesis with high temperature solid state synthetic method was carried out according to the following reaction:

$$Fe_2O_3 + 2V_2O_5 + V_2O_3 \rightarrow 2FeV_3O_8$$

However, following stoichiometric reactions could not be obtained single phase of FeV_3O_8, made with VO_2 phase as impurity. After that, we had been trying synthesis conditions changing temperature, atmosphere and the ratio of starting material based on $Fe_xV_{1-x}O_2$ ($0 \leq x \leq 0.5$). Finally, we could design perfect synthesis conditions ($x = 0.275$, Temperature: 800℃, Atmosphere: vacuum sealing state, quenching method: water quenching) and expressed according to the modified reaction:

$$1.1Fe_2O_3 + 2V_2O_5 + 0.9V_2O_3 \rightarrow 2Fe_{1.1}V_{2.9}O_8$$

The phase of the synthesized $Fe_{1.1}V_{2.9}O_8$ was investigated with the powder X-ray Rietveld refinement as presented in Figure. 4a with SEM image (Figure. 4b). The particle morphologies look like a chopstick and size of long axis is about 70um. The XRD refinement pattern for the pristine powder concurs with the reference CIF pattern of FeV_3O_8 (ICSD-30054), identifying the absence of any secondary phases that powder made well.

The crystal structure of $Fe_{1.1}V_{2.9}O_8$ is monoclinic with the space group of C 2/m and the lattice parameters were refined as a = 12.0938 Å, b= 3.6710 Å, c= 6.5268 Å $\beta = 106.86^\circ$. The refined atomic information and selected interatomic distances are summarized in the Table 1 and 2.

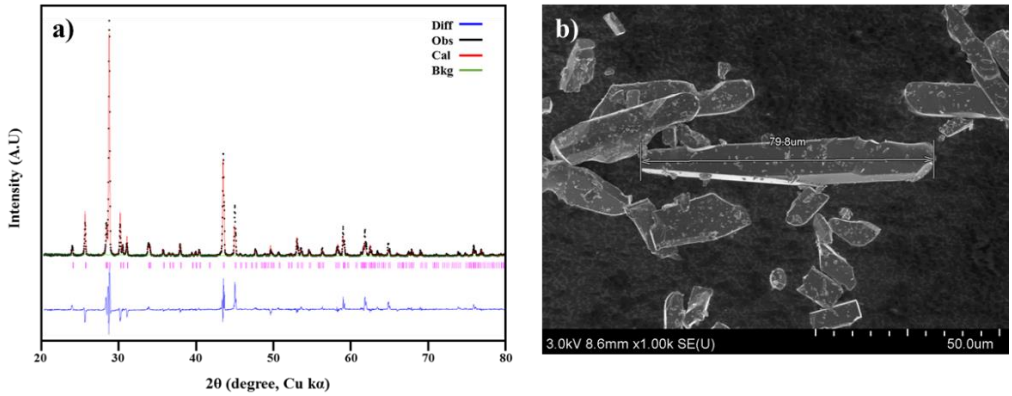

Figure 4 a) Observed and calculated X-ray Rietveld refinement profile for the $Fe_{1.1}V_{2.9}O_8$, recorded at room temperature (black line-experimental data, red line-calculated data, blue line-difference). b) FE-SEM image of the $Fe_{1.1}V_{2.9}O_8$ particles by high temperature solid state synthetic method

Figure 4b shows such particle morphology of $Fe_{1.1}V_{2.9}O_8$ contains a large size of plate-shape powder with long diffusion path, which expected occurring movement of lithium ion with high ionic conducting resistance. In order to exhibit better performances of electrochemical profiles, particle morphologies have to be pulverized to small size until submicron size to reduce the resistance of ion diffusion.

Table 1 Crystallographic data and Rietveld refinement results for FeV_3O_8 by powder XRD data

Crystal System			**Monoclinic**		
Space Group			**C 2/m**		
Lattice Parameter			**a = 12.0938 Å, b = 3.6710 Å, c = 6.5268 Å** **β = 106.86°, V = 289.8 Å^3, Z = 2**		
Atoms	**x**	**y**	**z**	**Mult**	**Occupancy**
Fe1	**0.30749(4)**	**0**	**0.72232(7)**	**4i**	**0.5**
V1	**0.39847(4)**	**0**	**0.30474(7)**	**4i**	**1**
V2	**0.30749(4)**	**0**	**0.72232(7)**	**4i**	**0.5**
O1	**0.3678(2)**	**0**	**0.9882(3)**	**4i**	**1**
O2	**0.2323(2)**	**0**	**0.3438(3)**	**4i**	**1**
O3	**0.4404(2)**	**0**	**0.6308(3)**	**4i**	**1**
O4	**0.1389(2)**	**0**	**0.7108(3)**	**4i**	**1**

*$R_p = 0.2376, R_{wp} = 0.2885, R_{exp} = 0.1626, R(F^2) = 0.27885, \chi^2 = 3.148$

Table 2 Selected bond lengths (Å) results for FeV_3O_8 by powder XRD data

Fe1-O1	**1.67601(5)**	**V2-O2**	**2.37211(7)**	**O3-V1**	**2.03960(6)**
Fe1-O2	**2.37211(7)**	**V2-O2**	**1.91477(8)**	**O3-V1**	**1.87047(6)**
Fe1-O2	**1.91477(8)**	**V2-O3**	**1.87020(5)**	**O3-V2**	**1.87020(5)**
Fe1-O3	**1.87020(5)**	**V2-O4**	**2.01837(6)**	**O4-Fe1**	**2.01837(6)**
Fe1-O4	**2.01837(6)**	**O1-Fe1**	**1.67601(5)**	**O4-V1**	**1.88600(8)**
V1-V1	**2.98254(9)**	**O1-V1**	**1.99031(6)**	**O4-V2**	**2.01837(6)**
V1-V2	**3.05766(7)**	**O1-V2**	**1.67601(5)**		
V1-O1	**1.99031(6)**	**O2-Fe1**	**2.37211(7)**		
V1-O2	**2.09784(6)**	**O2-Fe1**	**1.91477(8)**		
V1-O3	**2.03960(6)**	**O2-V1**	**2.09784(6)**		
V1-O3	**1.87047(6)**	**O2-V2**	**2.37211(7)**		
V1-O4	**1.88600(8)**	**O2-V2**	**1.91477(8)**		
V2-O1	**3.05766(7)**	**O3-Fe1**	**1.87020(5)**		

3.2 Electrochemical characterizations

We fabricated lithium ion cells in 2036 coin cells, consisting with a lithium metal as an anode and $Fe_{1.1}V_{2.9}O_8$ as a cathode and all electrochemical measurements were conducted at room temperature. The first discharge/charge cycle of $Fe_{1.1}V_{2.9}O_8$ electrode, where the initial open circuit voltage (OCV) was 2.75V (vs. Li^+/Li), in 1M $LiPF_6$ in EC/DMC (vol% 1:2) with the constant current of 0.2C (1C=79.5mAh g^{-1}) is presented in Figure 5a. Such reversible electrochemical reactions as can be showed following equation (1).

$$x\mathrm{Li}^+ + \mathrm{Fe}_{1.1}\mathrm{V}_{2.9}\mathrm{O}_8 + x\mathrm{e}^- \rightleftarrows \mathrm{Li}_x\mathrm{Fe}_{1.1}\mathrm{V}_{2.9}\mathrm{O}_8 \qquad (1)$$

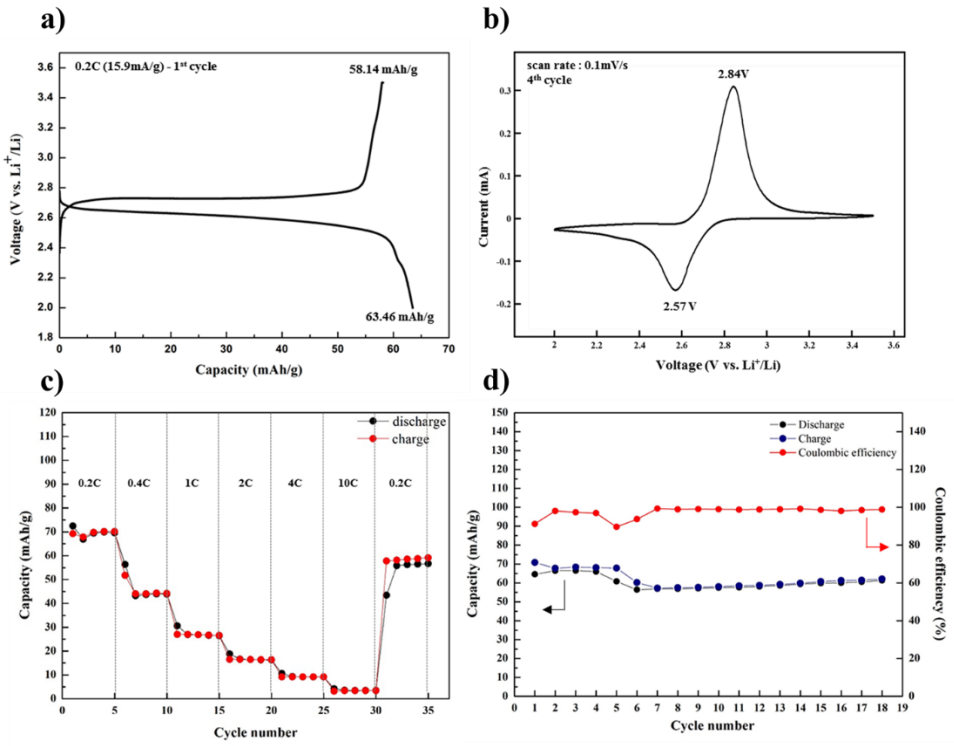

Figure 5 Electrochemical features of Li / 1M $LiPF_6$ in EC/DMC (vol% 1 : 2) / $Fe_{1.1}V_{2.9}O_8$ electrode Li-ion half cell ; a) constant current discharge/charge curve at 0.2C ; b) cyclic voltammetry curve in the voltage of 2-3.5 V ; c) rate performance at different current densities ; d) cycling performance and corresponding coulombic efficiency at a current of 15.9 mA g^{-1}

According to other reports by Murphy et al., lithium ion could be accommodated until in the framework of FeV_3O_8 until $Li_2FeV_3O_8$ by using chemical insertion with n-buLi. If lithium ion could be intercalated reversibly until 2, the theoretical specific capacity is 159 mAh g^{-1}. No workers, however, have been reporting lithium ion intercalation with 2 lithium ion, furthermore electrochemical profiles of FeV_3O_8 structure. In terms of our discharge/charge test, specific discharge capacity at first cycle delivers 63.46 mAh g^{-1} at 0.2C (1C=79.5mAh g^{-1}), which is far lower than the expected specific capacity (159 mAh g^{-1}). The galvanostatic profile exhibits one voltage plateau with the well-expected voltage range near 2.7V occurring redox reaction of 0.8 Li-ion insertion.

Figure 5b clearly presents the cyclic voltammetry profiles in the range of 2.0 - 3.5 V at fourth cycle of the $Fe_{1.1}V_{2.9}O_8$ electrode, which has two peaks in terms of oxidation and reduction reactions. Each peak points (oxidation peak & reduction peak) of such profile were matched with plateau range of discharge/charge curve.

Figure 5c shows that the rate capability of $Fe_{1.1}V_{2.9}O_8$ electrode could be identified tendency of capacity with different current densities. The specific capacity drastically decreases with increasing current density and shows specific capacity of 5 mAh g^{-1} at 10C.

Figure 5d shows that the cyclability test of the lithium cell with $Fe_{1.1}V_{2.9}O_8$ electrode at 0.2C. The stable reversible specific capacity of 58 mAh g^{-1} exhibit after 6 cycle and a high coulombic efficiency closed to 99% has been checked by following experiment.

The results obtained by electrochemical cell tests indicate that $Fe_{1.1}V_{2.9}O_8$ electrode could be operated well intercalation reaction of Li-ion in lithium half-cells with lithium metal, conventional electrolyte and $Fe_{1.1}V_{2.9}O_8$ as a cathode. Many factors were influenced to exhibit such electrochemical profiles. To further understand the electrochemical properties of $Fe_{1.1}V_{2.9}O_8$ electrode as cathode, the structural changes of the electrode before and after discharging at constant current density by using ex-situ XRD.

4. Conclusions

In summary, we investigated how lithium ion intercalation reaction were occurred into the FeV_3O_8 with structural and electrochemical studies. The tunnel structure of FeV_3O_8 (monoclinic, C2/m, a = 12.129(3) Å , b = 3.679(1) Å , c = 6.547(2) Å , β= 106.86°, V = 279.6 Å^3, Z = 2) as cathode has been applied to examine lithium ion intercalation test with a lithium half cell system. The FeV_3O_8 powder was prepared by high temperature solid state synthetic method with mixing precursors such as Fe_2O_3, V_2O_5 and V_2O_3. However, calculated stoichiometric composition with right numerical values were made with VO_2 phase as impurity. Therefore, we had been trying synthesis conditions to make single phase without impurity changing temperature, atmosphere and the ratio of starting material based on $Fe_xV_{1-x}O_2$ ($0 \leq x \leq 0.5$). Finally, we got a synthesis condition of FeV_3O_8 perfectly, such condition demonstrates following summarized sentence:

[$Fe_xV_{1-x}O_2$ ($0 \leq x \leq 0.5$) : $Fe_{1.1}V_{2.9}O_8$ (x = 0.275), Temperature: 800℃ , Atmosphere: vacuum sealing state with fused-silica tube, quenching method: water quenching]

The $Fe_{1.1}V_{2.9}O_8$ was synthesized the method of high temperature solid state reaction in vacuum sealed fused-silica tube for 36 hours at 800℃ (increase time: 10 hours). The evidences of the lithium ion movement with intercalation reaction into the host material $Fe_{1.1}V_{2.9}O_8$ shows such electrochemical tests as observed in the galvanostatic profiles and cyclic voltammetry (CV) curve in the voltage range of 2.0 - 3.5 V (vs. Li^+/Li). In the galvanostatic curve, specific discharge capacity at first cycle which is insertion process to $Li_xFe_{1.1}V_{2.9}O_8$ exhibits 63.46 mAh g^{-1} at 0.2C with having one voltage plateau near 2.7 V. According to CV data in voltage range of 2.0 - 3.5 V, the $Fe_{1.1}V_{2.9}$ O_8 electrode has two peaks as an oxidation peak (2.84 V) and a reduction peak (2.57 V) with electrochemical redox reactions. Each peak points from CV profile were confirmed with one voltage plateau range of galvanostatic curve. The reversible capacity of $Fe_{1.1}V_{2.9}O_8$ also decreases with increasing current density, showing the intercalation/de-intercalation behavior. Eventually, discharge capacity at 10C shows 5 mAh g^{-1}. The reversible specific capacity of $Fe_{1.1}V_{2.9}O_8$ could be investigated showing specific capacity of 58 mAh g^{-1} after 6 cycles and exhibits high coulombic efficiency above to 99%. While we have investigated electrochemical measurements of the $Fe_{1.1}V_{2.9}O_8$ cathode for Li-ion cells, several solutions to increase performances of the Li cell have to be considered.

요약문

리튬이차전지 양극 물질 개발을 위한 FeV_3O_8의 구조 및 전기화학분석

터널형상의 확산경로를 가진 단사정계형 FeV_3O_8 물질의 리튬이온 탈-삽입여부에 대한 전기화학적 실험을 진행하였다. 고온에서의 고체합성 방법을 이용하여 판상형 FeV_3O_8 분말을 획득 할 수 있었으며, XRD와 SEM을 이용하여 합성 여부와 형상을 파악하였다. 리튬 탈삽입 여부를 확인하기 위해 XRD를 이용한 구조적 실험과 Cyclic voltammetry와 galvanostatic discharge/charge curve를 이용한 전기화학적 실험을 진행하였다. 비록, 전기자동차를 충분히 가동시킬 수 있는 우수한 리튬이차전지 성능을 도출해내지는 못하였지만, 위 연구를 통해 FeV_3O_8 분말이 양극소재로써 활용될 가능성이 있음을 확인하였다. 안정한 양극물질로써, FeV_3O_8은 첫번째 방전곡선의 특정 용량 값이 63.51 mAh g^{-1} 로 전기화학적 산화-환원 반응을 동반하여 작동하였다. 2.0 - 3.5 V 전압범위 내 2.7 V 에서 FeV_3O_8 전극은 평평한 전압영역을 보였고, 순환효율은 99%에 근접하여 우수한 사이클 특성을 보여주었다. 불행히도, FeV_3O_8 전극은 좋지 못한 전류 속도 성능을 발휘하였고, 10C 에서의 방전용량이 5 mAh g^{-1} 의 수치를 보였다. 이러한 현상은 뚜렷한 판상형태를 가진 입자의 결정성이 리튬이온의 이동에 저항의 역할을 하는 것으로 판단된다.

우리는 FeV_3O_8 전극이 우수한 성능을 구현하기 위해 여러가지 추가 실험을 진행해야 한다. 전극 물질 내의 물리적, 화학적 특성을 향상 시키기 위해, 입자의 크기와 형상의 변화를 줄수 있는 실험들을 고려해야한다. 또 다른 예로 입자 위에 추가적인 코팅공정 등을 통해 리튬이온의 전도성을 향상시킬 수도 있다.

핵심어 : 단사정계 FeV_3O_8, 터널 형상 구조, 1차원 확산경로, 양극물질

References

1. Tarascon, J. M. & Armand, M. Issues and challenges facing rechargeable lithium batteries. *Nature* **414,** 359–367 (2001).

2. Braun, P. V, Cho, J., Pikul, J. H., King, W. P. & Zhang, H. High power rechargeable batteries. *Curr. Opin. Solid State Mater. Sci.* **16,** 186–198 (2012).

3. Aurbach, D. Review of selected electrode-solution interactions which determine the performance of Li and Li ion batteries. *J. Power Sources* **89,** 206–218 (2000).

4. Amatucci, G. Cobalt dissolution in LiCoO2-based non-aqueous rechargeable batteries. *Solid State Ionics* **83,** 167–173 (1996).

5. ZACHAUCHRISTIANSEN, B. Lithium insertion in different TiO2 modifications. *Solid State Ionics* **28-30,** 1176–1182 (1988).

6. Kerisit, S., Rosso, K. M., Yang, Z. & Liu, J. Computer Simulation of the Phase Stabilities of Lithiated TiO2 Polymorphs. *J. Phys. Chem. C* **114,** 19096–19107 (2010).

7. Wilkening, M., Lyness, C., Armstrong, A. R. & Bruce, P. G. Diffusion in Confined Dimensions: Li+ Transport in Mixed Conducting TiO2−B Nanowires. *J. Phys. Chem. C* **113,** 4741–4744 (2009).

8. Armstrong, A. R., Armstrong, G., Canales, J. & Bruce, P. G. TiO2–B nanowires as negative electrodes for rechargeable lithium batteries. *J. Power Sources* **146,** 501–506 (2005).

9. WHITTINGHAM, M. S. Electrical Energy Storage and Intercalation Chemistry. *Sci.* **192 ,** 1126–1127 (1976).

10. Chung, S. Y., Bloking, J. T. & Chiang, Y. M. Electronically conductive phospho-olivines as lithium storage electrodes. *Nat Mater* **1,** 123–128 (2002).

11. Barboux, P., Tarascon, J. M., Shokoohi, F. K. & Bank, R. The Use of Acetates as Precursors for the Low-Temperature Synthesis of LiMn , O , and LiCoO , Intercalation Compounds. *J. Solid State Chem.* (1991).

12. Wang, H., Jang, Y., Huang, B., Sadoway, D. R. & Chiang, Y. TEM Study of Electrochemical Cycling-Induced Damage and Disorder in LiCoO2 Cathodes for Rechargeable Lithium Batteries. *J.*

Electrochem. Soc. **146 ,** 473–480 (1999).

13. Amatucci, G. & Tarascon, J. M. Optimization of Insertion Compounds Such as LiMn[sub 2]O[sub 4] for Li-Ion Batteries. *J. Electrochem. Soc.* **149,** K31 (2002).

14. Zhang, X. *et al.* LiFePO4/NaFe3V9O19/porous glass nanocomposite cathodes for Li+/Na+mixed-ion batteries. *J. Mater. Chem. A* **3,** 22247–22257 (2015).

15. Murphy, D., Greenblatt, M., Cava, R. & Zahurak, S. Topotactic lithium reactions with ReO3 related shear structures. *Solid State Ionics* **5,** 327–329 (1981).

16. Muller, J., Joubert, J. C. & Marezio, M. Synthese et structure cristalline d'un nouvel oxyde mixte 'FeV3O8' (FexV1-xO2; x~0.25). *J. Solid State Chem.* **27,** 191–199 (1979).

17. Cava, R., Santoro, a, Murphy, D., Zahurak, S. & Roth, R. Structural aspects of lithium insertion in oxides: LixReO3 and Li2FeV3O8. *Solid State Ionics* **5,** 323–326 (1981).

18. Eibschütz, M. The effect of lithium on the electronic configuration of LixFeV3O8 (0≤x≤2). *Appl. Phys. Lett.* **39,** 664 (1981).

19. Cava, R. J., Santoro, A., Murphy, D. W., Zahurak, S. & Roth, R. S. The structures of lithium inserted metal oxides: Li2FeV3O8. *J. Solid State Chem.* **48,** 309–317 (1983).

20. Cava, R. J., Santoro, a., Murphy, D. W., Zahurak, S. M. & Roth, R. S. The structures of the lithium inserted metal oxides Li0.2ReO3 and Li0.36WO3. *J. Solid State Chem.* **50,** 121–128 (1983).

21. Hotta, Y. *et al.* Pressure-Products Diagram System. **04,** (1984).

22. Li, Y., Sun, C. & Goodenough, J. B. Electrochemical Lithium Intercalation in Monoclinic Nb12O29. *Chem. Mater.* **23,** 2292–2294 (2011).

※ Appendix

Structural and electrochemical studies on magnesium ion intercalation into NASICON and NASICON-like structure, $NaV_2(PO_4)_3$ and $V_2(PO_4)_3$.

Abstract

We investigate how affected by intercalation chemistry of magnesium ion into NASICON and NASICON-like structure. By using solution mixing with oxalic process, submicron sized $Na_3V_2(PO_4)_2$ and $Li_3V_2(PO_4)_3$ powder could be obtained and then, confirm powder phase, morphology and thermal stability by using SEM, XRD, TG analysis. To begin with, carrier metal ions were removed into the synthesized-powder by chemical extraction using I_2. We could not meet, however, reaction conditions proceeding magnesium intercalation test. Here, using electrochemical extraction method, experimental condition to obtain the host materials were successfully obtained for measuring magnesium intercalation test. The electrodes were fabricated before electrochemical test.

In order to determine magnesium ion intercalation profiles into those structure, cyclovoltammetry, galvanostatic discharge/charge curve and XRD analysis were conducted. Although magnesium rechargeable battery could be operated well were not developed within a given period of time, we discovered possibility of those materials through structural and electrochemical studies during project. Several countermeasures for magnesium ion intercalation were needed, however, to improve kinetic properties of materials. Above all, particle size control has to be considered and then, coating process onto particles surface using carbon or conducting material could be increased profiles of kinetic into the host materials. The next thing is to find conditions of the chemical extraction process without electrochemical extraction method. As a pre-process experiment for Mg ion intercalation, electrochemical extraction have critical bad influence on electrode surface. Contrary to existing reports, we demonstrate NASICON structure have possibility of Mg intercalation as a cathode material as mentioned above additional process for increasing kinetic of powder.

Keyword: Submicron-sized $NaV_2(PO_4)_3$ and $V_2(PO_4)_3$, Home-mad cell, activated carbon, chemical extraction, electro-chemical extraction.

Introduction

Recently, Lithium based rechargeable batteries have emerged as the significant area for portable power sources in the modern society [1]. Moreover, Future power hybrid vehicles and electric vehicles (EV) area are needed to large energy density (500Wh/kg) to be competitive in driving range and cost to vehicles powered by combustion engines [4]. Lithium-based rechargeable batteries are, however, being almost reached theoretical energy density (300Wh/kg) that is insufficient requirements for EV system. In addition, the sources of lithium have limited to specific area as poorly accessible forms, *e.g.* 0.04-1.16% in brine ponds, which require about 1 year for the final production of lithium carbonate [2]. Moreover, lithium-based metal is not environmentally friendly, safe and therefore, there is a need for high recycling costs or proper disposal to prevent dissemination of the toxic elements into the environment. As a result, the new concept of energy storage in electrical power applications of the future have to be essentially developed due to their various technical and cost barriers as well as the inherent safety and growing environmental concern [3].

Herein, we have been studied that one of the post-Li ion batteries, magnesium-based rechargeable batteries, have been receiving increasing attention to satisfy the use of power sources based on natural abundant materials. The merits of magnesium based rechargeable batteries are theoretical high volumetric capacity as well as inexpensive and high safety to handle than lithium based rechargeable batteries (※*3833 mAh/cc for Mg vs. 2046 mAh/cc for Li*). These characteristics can be utilized future stationary ESS and EV applications [2, 3].

Magnesium based rechargeable batteries have been in its early states to be commercialized. Magnesium re-chargeable batteries are based on the similar principle as Li-ion rechargeable batteries with regard to intercalation chemistry and cell configurations. Several difference such as interface mechanism into electrode/electrolyte are, however, occurred in contrast with lithium ion rechargeable batteries. There are so many assignments accumulated that we have to solve the problems [1-3]. We made mention of some examples of these problems at below. Magnesium intercalation chemistry suffers from several serious limitations contrary to lithium intercalation chemistry: (ⅰ) hindrance in diffusion of the multivalent Mg-ion in oxide-based electrode systems compared to the monovalent Li-ion [4]. The diffusion energy of magnesium into ox-ide-based electrode materials have much required than lithium ion because of highly Mg-O bonding energy relations. (ⅱ) the growth of an insulating

passivation surface film on the Mg-metal anode that makes the electrodes useless electrochemically with the commonly used organic salt and solution (*e.g.* salts ($Mg(ClO_4)_2$, $Mg(SO_3CF_3)_2$, and $Mg(N(SO_2CF_3)_2)_2$), solutions(carbonate and nitriles) [2]. These phenomenon lead to critical disadvantage that could not be used Mg metal and finally, (ⅲ) the absence of appropriate electrolytes which have wide electrochemical window for high voltage Mg-ion rechargeable batteries [16]. Researchers in the field of Mg battery have to develop non-aqueous electrolytes which could be operated with magnesium metal anode system.

In 2000, the first breakthrough works of Mg battery are reported by Aurbach's group [1]. A two aspects what they reported has emerged as innovative energy storage devices replace lithium source with magnesium source. First, the new concept of electrolyte system which magnesium metal could be used was developed. When electrochemical reactions were occurred on magnesium metal, Mg metal does not make dendrite formations in contrast with lithium-metal. Second, overcoming the high diffusion energy of magnesium into conventional cathode electrode, they suggest a promising cathode material that could be capable of intercalation/de-intercalation reaction. Start with this report, some groups have been studied magnesium-based energy storage with various sights [1].

Although this report could not be commercialize of Mg battery area and have still a long way to go, it suggest various start of magnesium-based battery research in the domain of post Li-ion battery. In addition, many researchers who have interested in magnesium-based rechargeable battery may take a direction which parts are more suitable for one's specialty. Cathode materials, one of the part of Mg battery, are received the attention to many researchers in the field of material scientist or inorganic chemists.

Until now, several groups suggest for cathode electrode candidates such as Chevrel phases $M_xMo_6T_8$ (M=metal, T=S,Se) [10], vanadium oxides [11,12], TiS_2 nanotubes [13] and graphite like MoS_2 [14]. However, these materials are still not suitable to develop high voltage materials. Herein, we investigate the development of cathode electrode material with higher operational voltage. Our research direction look face to goal of ① as shown in Figure. 1

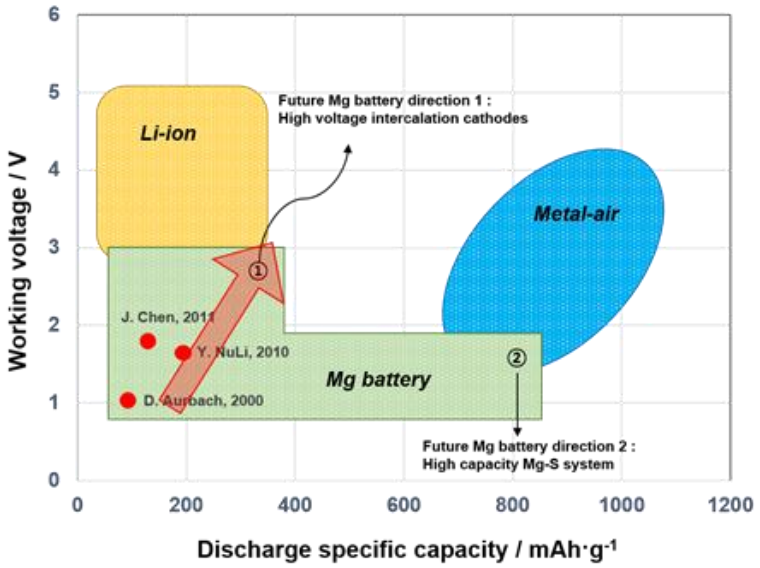

Fig. 1 Schematic of working voltage and specific capacity of Mg battery compared with other energy storage devices. [2]

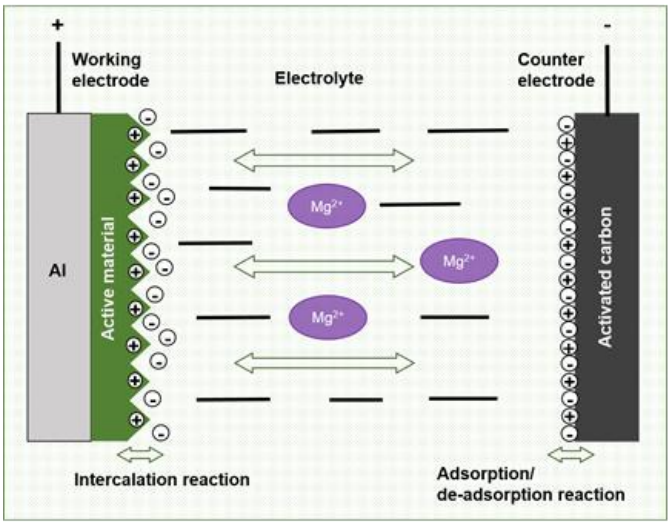

Fig. 2 Reaction mechanisms of hybrid cell in home-made cell configuration

To investigate our research purpose, we have not selected using magnesium metal but designed new concept of cell configuration. The detail design of new-type cell (called to hybrid cell) is shown as Figure. 2. We could check, therefore, electrochemical characterization whether cathode could operate or not in Mg-ion intercalation system.

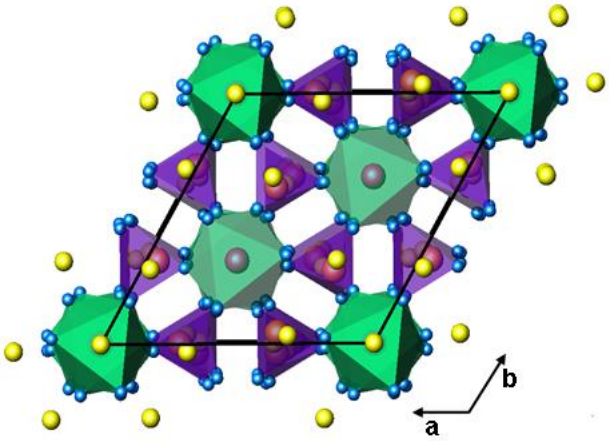

Fig. 3 A crystal structure of rhombohedra $Na_3V_2(PO_4)_3$

NASICON is a short for Na Super Ionic Conductor. One of the NASICON-type material, $Na_3V_2(PO_4)_3$ material; these materials are known for their facile sodium ion conductivity due to highly covalent open 3D frame-work crystalline structure with large tunnels [8]. $Na_3V_2(PO_4)_3$ has and rhombohedra unit cell with the space group of R-3c, cell parameters a=8.7288Å b=8.7288Å. c=21.8042Å and then, schematic crystal structure has shown in Figure. 3 [9].

In these properties, it have received attention in the field of sodium based solid electrolyte candidate. Moreover, NVP is employed to accommodate the lots of sodium ions for small-structure-changed intercalation process and therefore, it can be used applied cathode electrode materials for sodium-ion rechargeable batteries. In principle, NVP could present two different types of Na sites (6b,M1 and 18e, M2) that can be distinguished during intercalation/de-intercalation reaction between $Na_3V_2(PO_4)_3$ and $NaV_2(PO_4)_3$. When Na is extracted from $Na_3V_2(PO_4)_3$ to $NaV_2(PO_4)_3$, only one Na site (6b, M1) is remained in $NaV_2(PO_4)_3$ [8].

In order to apply to the field of magnesium-based batteries, we investigate whether be utilized magnesium electrode material as a cathode or not. First of all, we carried out two types of sodium ion extraction process from $Na_3V_2(PO_4)_3$ to $NaV_2(PO_4)_3$ and then assemble the home-made cell configuration in non-aqueous Mg organic electrolyte. Next, we measured characterizations of electrochemical intercalation process with magnesium ion into $NaV_2(PO_4)_3$ host material. The detail process has shown Figure. 4

To understand the complex mechanism of magnesium electrochemical intercalation into $NaV_2(PO_4)_3$ structure, we have been extended the sight of structural aspect how structure changed during intercalation/de-intercalation process.

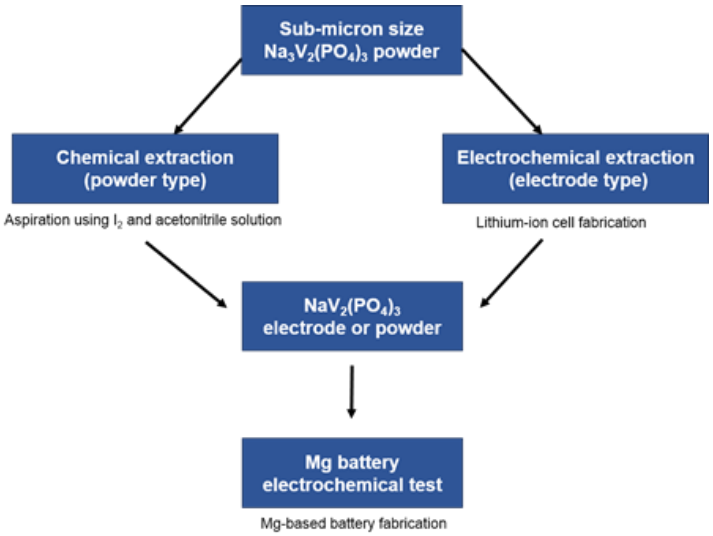

Fig. 4 A scheme of pre-processing experiment for NVP to fabricate Mg-ion cell

$Li_3V_2(PO_4)_3$ is one of the material which has monoclinic NASICON-like type structure also be called LISICON(Lithium super ionic conductor); it is known for their facile lithium ion conductivity due to similar structural properties of NASICON structure that has large tunnels. $Li_3V_2(PO_4)_3$ has and monoclinic unit cell with the space group of $P2_1/C$, cell parameters a=8.6017Å b=12.0717Å. c=8.5974Å and then, schematic crystal structure has shown in Figure. 5 [7].

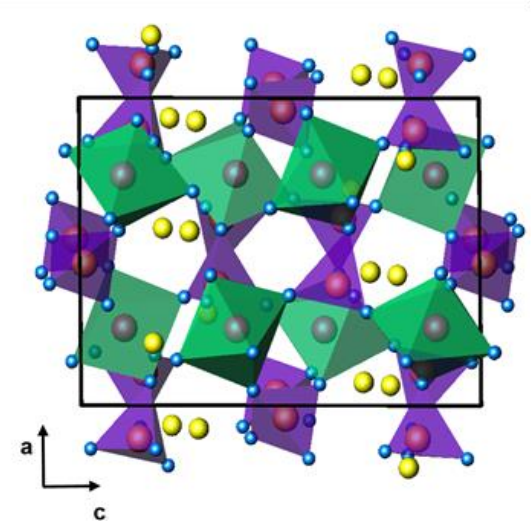

Fig. 5 A schematic crystal structure of monoclinic $Li_3V_2(PO_4)_3$

$Li_3V_2(PO_4)_3$ also have received attention in the field of lithium-ion battery as a prospective cathode material. This is because LVP could accompanies 3 Li^+ ions migration when electrochemical reaction go along. And then, it can be utilized higher capacity cathode material (theoretical capacity: 197.23mAh/g) for lithium-ion rechargeable batteries [17]. In order to measure of operating magnesium- batteries as a cathode, we conducted same method by two types of extraction like a NVP extraction method.

First of all, we carried out two types of lithium ion extraction process from $Li_3V_2(PO_4)_3$ to $V_2(PO_4)_3$ and then assemble the home-made cell configuration in non-aqueous Mg organic electrolyte. To conduct Mg intercalation experiments, several pre-treatment process need to proceed. Overall experimental process and research sight of Mg batteries are same with $Na_3V_2(PO_4)_3$ only difference of species and extracted ions quantity.

Experimental section

$Na_3V_2(PO_4)_3$

Submicron-sized $Na_3V_2(PO_4)_3$ compound was synthesized by using solution mixing method with oxalic process. Stoichiometric amounts of Na_2CO_3 (Aldrich, 99.5%), V_2O_5 (Aldrich, 99.6%), and $(NH_4)_2HPO_4$ (KANTO, 99%) with molar ratio 3:2:6 were used as starting materials. (a) The precursor were mixed and stirred in distilled water before being calcination at 300℃ by forced-air drying. (b) When stirring state, oxalic powder (*e.g.* V_2O_5 : $C_2H_2O_4$ □$2H_2O$ = 1:3 mole ratio) was inserted into mixing solution to reduce the powder particle size [15]. (c) After completely drying the sample, the precursor was ground and calcination at 300℃ in an air state for 4 hours (increase time: 2hours), reground, and (d) fired at 930℃ for 8h (increase rate: 2℃/min) under a flow of H_2 atmosphere. The details are referred to schematic as shown in figure. 6

$Li_3V_2(PO_4)_3$

Submicron-sized $Li_3V_2(PO_4)_3$ compound was synthesized similar with NVP method by using solution mixing method with oxalic process. (a) Stoichiometric amounts of Li_2CO_3 (Aldrich, 99.0%), V_2O_5 (Aldrich, 99.6%), and $(NH_4)_2HPO_4$ (KANTO, 99%) with molar ratio 3:2:6 were used as starting materials. (b) The precursor were mixed and stirred in distilled water by air drying before being calcination at 300℃. When stirring state, oxalic powder (e.g. V_2O_5 : $C_2H_2O_4$□$2H_2O$ = 1:3 mole ratio) was inserted into mixing solution to reduce the powder particle size[15]. (c) After completely drying the sample, the precursor was ground and calcination at 300℃ in an air state for 4 hours (increase time: 2hours), reground, and (d) fired at 850℃ for 8h (increase rate : 2℃/min) under a flow of H_2 atmosphere. The details came up to schematic above shown in Figure. 6

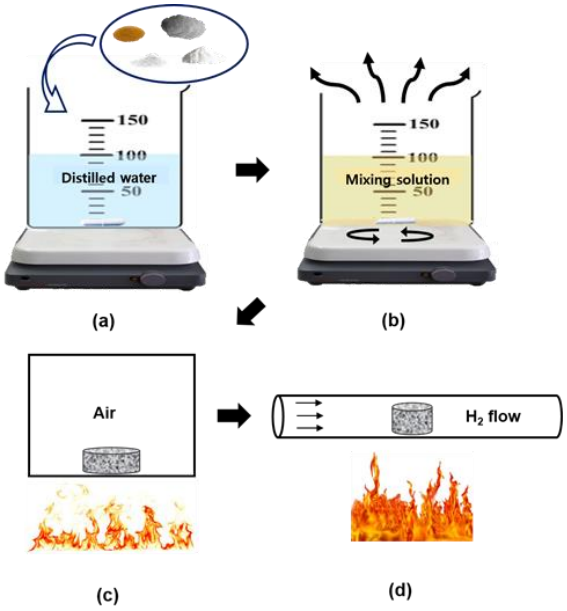

Fig. 6 A Synthesis process of $Na_3V_2(PO_4)_3$ or $Li_3V_2(PO_4)_3$powder; (a) preparation of precursors (b) mixing precursors with solution state (c) calcination process of pelletized-sample (d) final reaction process at gas flow atmosphere

XRD

The crystallographic structure of the as prepared material was studied by using XRD on a Miniflex 600 Rigaku with mono-chromatic CuK_α radiation (λ=1.5406Å), and the diffraction data were recorded in the 2θ range of 5-80° with a step size of 0.02° and a duration time of 0.5s. XRD refinements were performed using GSAS software.

Scanning Electron Microscope (SEM)

The particle morphology of the composite was investigated by using S-4800, HITACHI scanning electron microscope.

TG analysis

In order to measure thermal stability of active material, TG analysis of the samples was carried on a TG thermo-analyzer (Rigaku, TG8120).

Working electrode (NVP)

NVP electrodes were fabricated via a traditional pressed powder film method using submicron-size $Na_3V_2(PO_4)_3$. Electrodes slurry were made of active material (NVP), acetylene black, and binder (Polyvinyli-dene fluoride, PvdF) in a weight ratio of 7:2:1 dissolved in N-methyl-2-pyrrolidone using a Thinky mixer (Thinky). The slurry was coated onto 15um thick aluminum (Al) foil using a doctor blade and mini-coater (Hohsen). The coated electrodes pressed to a film thickness of 50um via a roller press (Wellcos Corporation) and then, were dried under vacuum at 120℃ for 24h and stored in an argon (Ar) filled glove box followed by drying in vacuum at 120℃ for 24h. The electrodes have a loading density of ~0.19mAh/cm^2, and porosity of ~52%.

Counter electrode

The counter electrodes were prepared in a form of pellets using a press, which were mixtures of activated carbon (Daejumg Chemicals & Metals) and poly(tetrafluoroethylene) (Sigma Aldrich) in a weight of 7 : 3.

Electrolyte

1M $Na(ClO_4)$ in propylene carbonate

In order to extract sodium ion from $Na_3V_2(PO_4)_3$, the electrolyte was fabricated in glove box putting 1M $Na(ClO_4)$ (ACS regent, Sigma Aldrich) in propylene carbonate (99.0%, Junsei). In order to treat about water pollutants, 1M $Na(ClO_4)$ salt was dried at 120℃ for 12h and then, PC solution took off a cover in Ar-filled glove box before mixing with solution and salt. Although water protect process are carried out, solution has still water pollutants about ~3000 ppm. It is hard to completely remove the water content from fresh PC solution contained large amount of water. For that reasons, we did conduct advanced water treatment by using zeolite mesh (200mesh, Wako) and molecular sieve (3A, Yakuri). After that, the solution in the bottles kept in the glove box for more than a day. The water contents of the finished dried electrolytes were about ~10ppm.

0.5M $Mg(ClO_4)_2$ in acetonitrile

The fabrication method and water treat process are similar with above mentioned. The differences are only initial salt and solution. The electrolyte was fabricated in glove box putting 0.5M $Mg(ClO_4)_2$ (ACS regent, Sigma Aldrich) in acetonitrile (99.8%, Samchun).

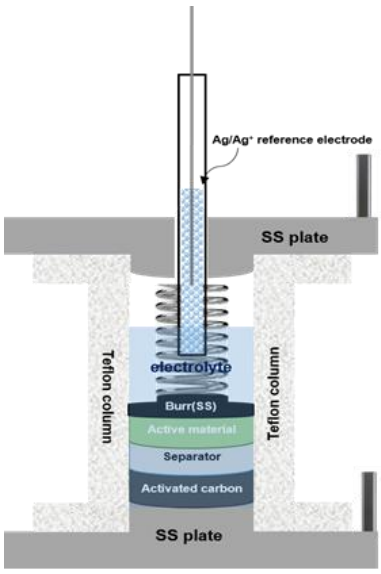

Fig. 7 Schematic of home-made cell configuration for operating Mg battery

Figure.7 described home-made cell configuration (called to K-cell) to evaluate cell test for measuring electro-chemical properties of cathode materials. K-cell was fabricated in a glove box with Ag/Ag^+ (0.01M $AgNO_3$ and 0.5M $Mg(ClO_4)_2$ in acetonitrile) as a reference electrode, the separator and activated carbon pellet as a counter electrode.

All electrochemical tests were conducted at room temperature in a glove box with less than 1 ppm of H_2O and O_2 contents.

Results and Discussion

$Na_3V_2(PO_4)_3$

In order to prepare the $Na_3V_2(PO_4)_3$ powders, synthesis method with oxalic process was carried out according to the following reaction:

$$3Na_2CO_3 + 2V_2O_5 + 6(NH_4)_2HPO_4 \rightarrow 2Na_3V_2(PO_4)_3$$

The XRD pattern of $Na_3V_2(PO_4)_3$ (NVP)powder is shown in Figure. 8 (a). The XRD pattern for the pristine powder concurs with the reference CIF pattern of $Na_3V_2(PO_4)_3$, identifying the absence of any secondary phases. XRD refinement data demonstrates convincingly result that powder made well.

In addition, synthesis with oxalic process was confirmed particles size with the SEM images shown in Figure. 8 (b), (c). NVP particles with normal solid-state-synthesis are almost agglomerated together to form larger clusters, by, contrast, particles morphology with oxalic process distinct from normal synthesis method. The average particles size of $Na_3V_2(PO_4)_3$ with oxalic process are about ~600nm.

Figure. 8b shows thermal stability of $Na_3V_2(PO_4)_3$ powder in the range of 25-350℃. Above 350℃, NVP powder occurred some reactions gaining weight of material with thermal absorption. Using galvanostatic sodium extraction method, $NaV_2(PO_4)_3$ was acquired successfully as shown in Figure. 8.

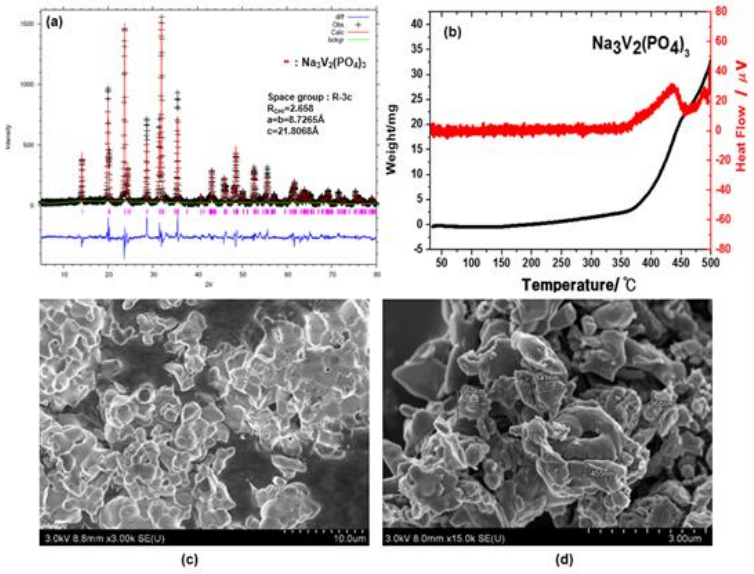

Fig. 8 (a) XRD refinement of $Na_3V_2(PO_4)_3$ powder by using GSAS program (b) TG analysis of $Na_3V_2(PO_4)_3$ (c) SEM image of $Na_3V_2(PO_4)_3$ by simple solid state synthesis and (d) with oxalic process

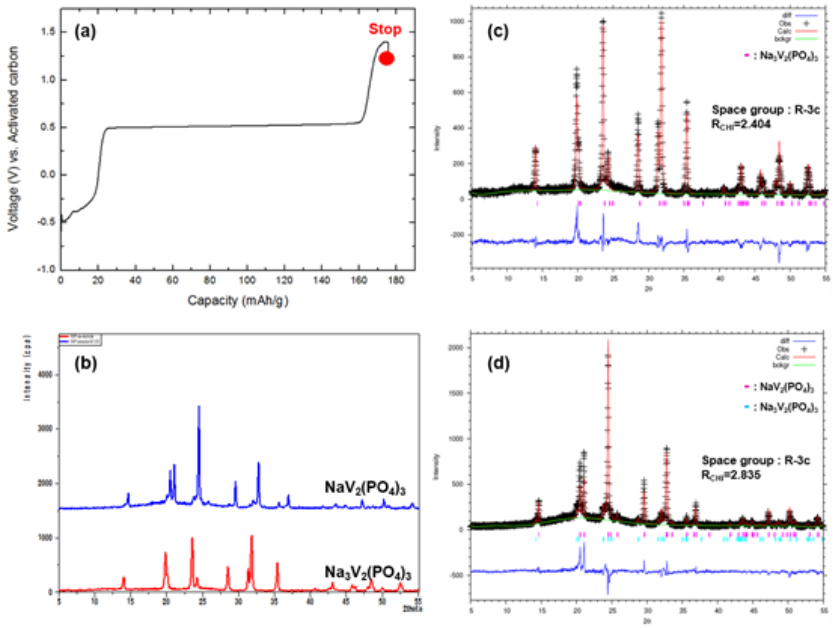

Fig. 9 (a) Galvanostatic sodium-extraction voltage profile from $Na_3V_2(PO_4)_3$ to $NaV_2(PO_4)_3$ (b) XRD patterns of $Na_3V_2(PO_4)_3$ and $NaV_2(PO_4)_3$ electrode (c) XRD refinement of $Na_3V_2(PO_4)_3$ electrode by GSAS software (d) XRD refinement of $NaV_2(PO_4)_3$ electrode by GSAS software.

The electrochemical curve (Fig.9a) show one of the evidence whether sodium ion extracted or not. Next, through a structural change (Fig.9d), it is confidently expected that $NaV_2(PO_4)_3$ was prepared properly.

XRD patterns are refined using Rietveld analysis by GSAS program as shown in Fig. 9c and Fig. 9d. Refinement

information of $Na_3V_2(PO_4)_3$ and $NaV_2(PO_4)_3$ made up lists with each atomic position and bonding distance in Table.1 and Table.2 ($Na_3V_2(PO_4)_3$) and Table.3 and Table.4 ($NaV_2(PO_4)_3$) and then, R factor are 2.404% and 2.835%. In addition, cell parameters of each material while electrochemical experiments from $Na_3V_2(PO_4)_3$ to $NaV_2(PO_4)_3$ were changed and then, unit cell volume also shrunk about ~8% as shown in Table. 5.

The structure in fig.9d shows that $NaV_2(PO_4)_3$ was not fabricated as a pristine phase but slightly contained $Na_3V_2(PO_4)_3$ phase. Nevertheless, we carried out magnesium insertion test obtained material by electrochemical extraction.

In order to extract sodium-ion in host materials, cathode electrodes were fabricated to conduct electrochemical experiments unlike a chemical extraction method. It was quite complicated pre-process before measuring magnesium ion intercalation test into $NaV_2(PO_4)_3$. According to other reports in the field of magnesium battery, interface mechanisms between electrode and electrolyte are extremely crucial to move magnesium ion into the host materials. Extraction process by electrochemical test is, however, affected surface of electrode while cell assembled/disassembled.

Table 1. Crystallographic data of the $Na_3V_2(PO_4)_3$ electrode at room temperature

Atom	Type	Wyckoff	x	y	z	Occupancy	UISO
Na1	Na^+	6b	0.3333	0.6667	0.1667	0.8050	0.0125
Na2	Na^+	18e	0.6667	0.9673	0.0833	0.7310	0.0125
V	V^{+3}	12c	0.3333	0.6667	0.0195	1.0000	0.0125
P	P	18e	-0.0427	0.3333	0.0833	1.0000	0.0125
O1	O^{-2}	36f	0.1419	0.4977	0.0776	1.0000	0.0125
O2	O^{-2}	36f	0.5405	0.8448	-0.0264	1.0000	0.0125

Table 2. Selected bon lengths (Å) of $Na_3V_2(PO_4)_3$ electrode

V1-Na1	3.20760(33)	Na1-O1	2.50243(18)	P1-O1	1.53495(13)
V1-Na2	3.10484(22)	Na1-O1	2.50211(18)	P1-O1	1.53466(13)
V1-Na2	3.10439(22)	Na1-O1	2.50266(18)	P1-O2	1.52123(11)
V1-Na2	3.10517(22)	Na2-V1	3.10484(22)	P1-O2	1.52249(11)
V1-O1	2.02575(13)	Na2-V1	3.10463(22)	O1-V1	2.02575(13)
V1-O1	2.02615(13)	Na2-Na1	3.31810(23)	O1-Na1	2.50349(18)
V1-O1	2.02547(13)	Na2-Na1	3.31651(23)	O1-Na2	2.38697(21)
V1-O2	1.96812(14)	Na2-P1	2.92006(25)	O1-Na2	2.44321(21)
V1-O2	1.96767(14)	Na2-P1	2.99457(26)	O1-P1	1.53495(13)
V1-O2	1.96841(14)	Na2-P1	2.92091(25)	O2-V1	1.96812(14)
Na1-V1	3.20760(33)	Na2-O1	2.44321(21)	O2-Na2	2.62575(23)
Na1-V1	3.20615(33)	Na2-O1	2.38697(21)	O2-Na2	2.83315(21)
Na1-Na2	3.31810(23)	Na2-O1	2.38655(21)	O2-P1	1.52123(11)
Na1-Na2	3.31769(23)	Na2-O1	2.44303(21)		
Na1-Na2	3.31841(23)	Na2-O2	2.62575(23)		
Na1-Na2	3.31648(23)	Na2-O2	2.83315(21)		
Na1-Na2	3.31575(23)	Na2-O2	2.83402(21)		
Na1-Na2	3.31606(23)	Na2-O2	2.62689(23)		
Na1-O1	2.50349(18)	P1-Na2	2.92006(25)		
Na1-O1	2.50382(18)	P1-Na2	2.92091(25)		
Na1-O1	2.50327(18)	P1-Na2	2.99457(26)		

Table 3. Crystallographic data of the $NaV_2(PO_4)_3$ electrode at room temperature

Atom	Type	Wyckoff	x	y	z	Occupancy	UISO
Na1	Na^+	6b	0.0000	0.0000	0.0000	1.0000	0.0125
V	V^{+4}	12c	0.0000	0.0000	0.0145	0.9583	0.0125
P1	P	18e	0.2870	0.0000	0.2500	1.0000	0.0125
O1	O^{-2}	36f	0.1760	-0.0250	0.1910	1.0000	0.0125
O2	O^{-2}	36f	0.1910	0.1640	0.0870	1.0000	0.0125

Table 4. Selected bon lengths (Å) of $NaV_2(PO_4)_3$ electrode

Na1-V1	3.1140(4)	Na1-O2	2.40112(21)	V1-O2	1.95600(17)
Na1-V1	3.1140(4)	Na1-O2	2.40112(21)	P1-Na1	3.51217(33)
Na1-P1	3.51217(33)	Na1-O2	2.40112(21)	P1-Na1	3.51217(33)
Na1-P1	3.51217(33)	Na1-O2	2.40112(21)	P1-O1	1.52552(14)
Na1-P1	3.51217(33)	V1-Na1	3.1140(4)	P1-O1	1.52552(14)
Na1-P1	3.51217(33)	V1-O1	1.87896(18)	P1-O2	1.51646(18)
Na1-P1	3.51217(33)	V1-O1	1.87896(18)	P1-O2	1.51646(18)
Na1-P1	3.51217(33)	V1-O1	1.87896(18)	O1-V1	1.87896(18)
Na1-O2	2.40112(21)	V1-O2	1.95600(17)	O1-P1	1.52552(14)
Na1-O2	2.40112(21)	V1-O2	1.95600(17)	O2-Na1	2.40112(21)
O2-V1	1.95600(17)	O2-P1	1.51646(18)		

Table 5. The comparison of crystallographic data of the $Na_3V_2(PO_4)_3$ and $NaV_2(PO_4)_3$ electrode at room temperature

Materials	a (Å)	b (Å)	c (Å)	α	β	γ	Volume (Å^3)
$Na_3V_2(PO_4)_3$	8.7232	8.7232	21.7905	90.0000	90.0000	120.0000	1658.13
$NaV_2(PO_4)_3$	8.4237	8.4237	21.4760	90.0000	90.0000	120.0000	1523.91

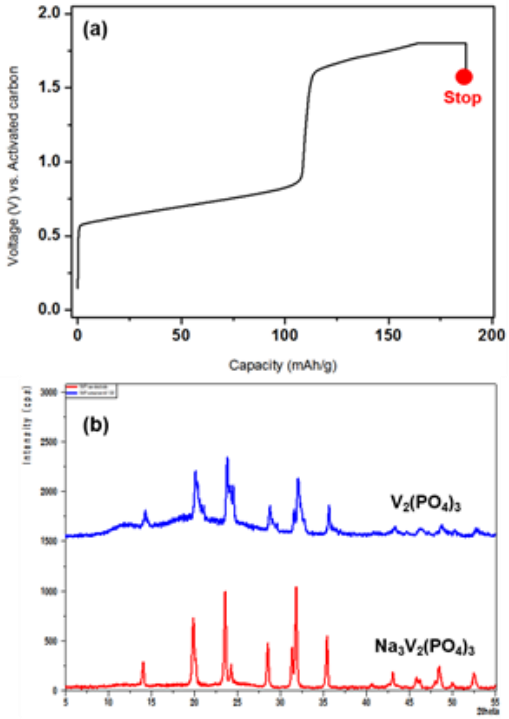

Fig. 10 (a) Over extraction of sodium-ion from $Na_3V_2(PO_4)_3$ to $V_2(PO_4)_3$ up to 1.8V by electrochemical extraction and (b) XRD patterns of $Na_3V_2(PO_4)_3$ and $V_2(PO_4)_3$

In general, $Na_3V_2(PO_4)_3$ have known two sodium intercalation range. If sodium ions were extracted changing into rhom-$V_2(PO_4)_3$, NASICON structure could be collapsed. We investigated how changed the structure when sodium extraction to excess. Figure. 10a shows galvanostatic voltage profile during sodium extraction. In potential range of 1.5V-1.8V, the curve appeared plateau reaction operating as a battery performance and XRD pattern was changed otherwise $NaV_2(PO_4)_3$ structure as shown in Figure 10b. Before conducting XRD patterns in Figure 10b, we believe that reversible plateau reaction could be applied high capacity sodium-ion battery or new candidate host material, rhom-$V_2(PO_4)_3$, for magnesium rechargeable batteries. XRD pattern of $V_2(PO_4)_3$ looks, however, becoming poor-crystalline structure that hard to utilize as a cathode material.

Before conducting magnesium ion intercalation test, default-type experiments of sodium-ion battery operation were investigated in our home-made cell system. We prepared an extraordinary component of our cell type, activated carbon, which has affected adsorption/de-adsorption reaction on surface as a principle of capacitor. Indeed, sodium ions rechargeable cell using activated carbon as a counter electrode were working normally confirming in Figure. 11a and 11b.

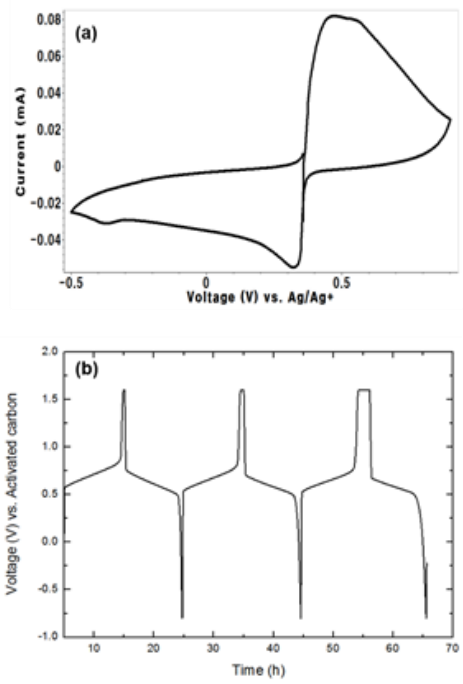

Fig. 11 (a) Cyclovoltammetry (CV) and (b) galvanostatic charge/discharge curves of $Na_3V_2(PO_4)_3$ in the home-made cell system

It is time to discuss the operation of magnesium ion intercalation with our cell system. Figure. 12 illustrates that Mg ion diffusion into $Na_3V_2(PO_4)_3$ with 0.5M $Mg(ClO_4)_2$ in acetonitrile has evolved with intercalation reaction, and confirming XRD patterns whether structure changed or not. In Figure. 12a, oxidation peak at CV curves has appeared due to sodium ion extraction. This is because pristine-$Na_3V_2(PO_4)_3$ electrode was fabricated. Unlike an oxidation peak, reduction peak as a signal of magnesium ion insertion has extremely reduced. After 1st cycle, we check the structural change using XRD pattern. In principle, $Na_3V_2(PO_4)_3$ and after 1^{st} cycle XRD patterns are same, provided reversible oxidation/reduction reactions were occurred. It is, however, different after 1 cycle as shown in Figure. 12b. That is, either magnesium ion or sodium ion could not be completely inserted into $NaV_2(PO_4)_3$ structure, nevertheless, as shown in Figure 12c, significant evidence that a small quantity of carrier ion were inserted into $NaV_2(PO_4)_3$ was caught. Even though structure was changed, it hard to understand which atoms inserted into the host structure.

To establish carrier metal ion into $NaV_2(PO_4)_3$ host, cyclovoltammetry test was conducted with 0.5M $Mg(ClO_4)_2$ as shown Figure. 12. In order to insert Mg-ion, electrochemical condition sets to reduction-first, though reduction peak was disappeared as shown in Figure. 13b. After that, oxidation peak would be seen putative sodium ion included $NaV_2(PO_4)_3$ compound. CV peak profiles eventually were reduced after few cycles as shown in Figure. 13d.

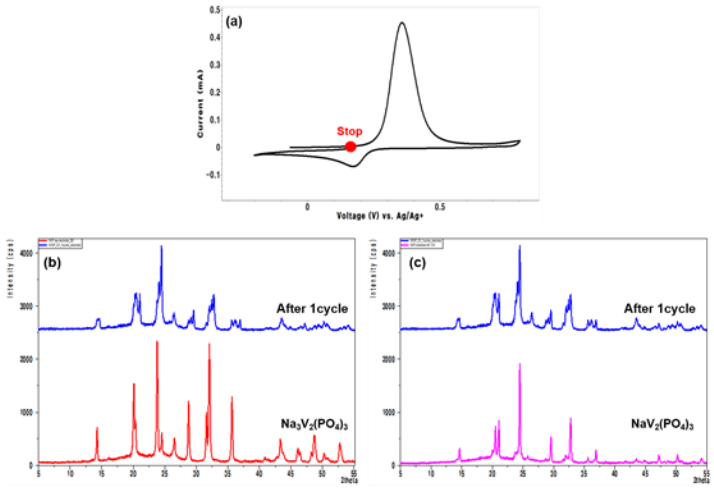

Fig. 12 (a) Cyclovoltammetry curve of $Na_3V_2(PO_4)_3$ with 0.5M $Mg(ClO_4)_2$ in acetonitrile (b) XRD patterns of $Na_3V_2(PO_4)_3$ and state of stop point in Figure. 12a (c) XRD patterns of $NaV_2(PO_4)_3$ and state of stop point in Figure. 15a

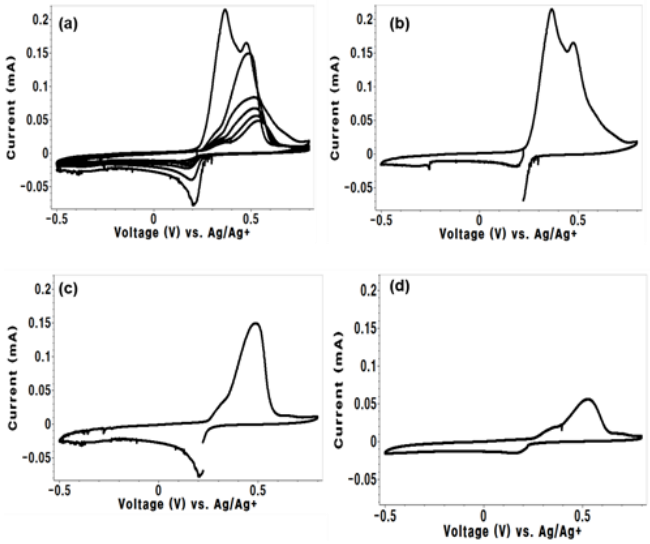

Fig. 13 The cyclovoltammetry test of $NaV_2(PO_4)_3$ (a) Overall cycle property and (b) 1^{st} cycle, (c) 2^{nd} cycle, (d) 5_{th} cycle with 0.5M $Mg(ClO_4)_2$ in acetonitrile

$Li_3V_2(PO_4)_3$

In order to prepare the $Li_3V_2(PO_4)_3$ powders, synthesis method with oxalic process was carried out according to the following reaction:

$$3Li_2CO_3 + 2V_2O_5 + 6(NH_4)_2HPO_4 \rightarrow 2Li_3V_2(PO_4)_3$$

The XRD pattern of $Li_3V_2(PO_4)_3$ (LVP)powder is shown in Figure. 14a. The XRD pattern for the pristine powder concurs with the reference CIF pattern of $Li_3V_2(PO_4)_3$, identifying clearly synthesis without contaminated phases. XRD refinement data demonstrates convincingly result that powder made well.

In the similar with $Na_3V_2(PO_4)_3$, material characterizations were investigated confirming particles size with the SEM images as shown in Figure. 14c, 14d.

Figure. 14b shows thermal stability of $Li_3V_2(PO_4)_3$ powder in the range of 25-350℃. Above 350℃, LVP powder lead to some reactions accompanying gaining weight and thermal exchange.

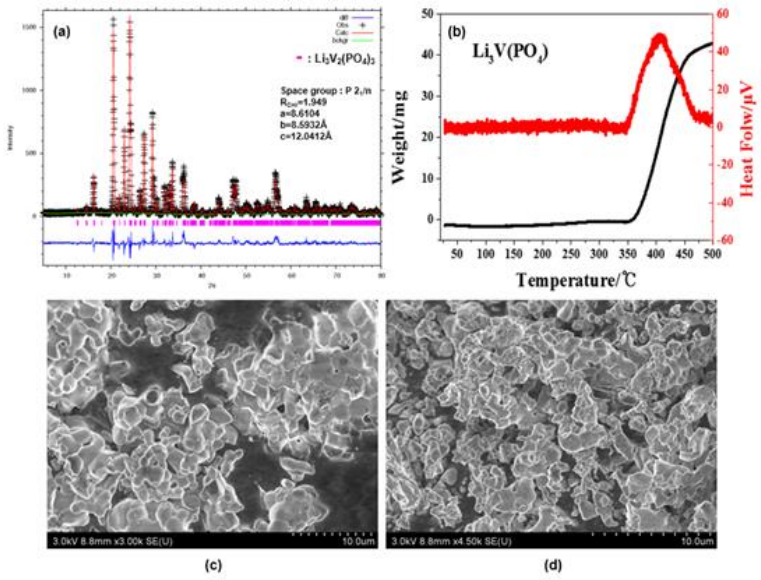

Fig. 14 (a) XRD refinement of $Li_3V_2(PO_4)_3$ powder by using GSAS program (b) TG analysis of $Li_3V_2(PO_4)_3$ (c) SEM image of $Li_3V_2(PO_4)_3$ by simple solid state synthesis (d) SEM image of $Li_3V_2(PO_4)_3$ with oxalic process

Implementing galvanostatic delithiation voltage profiles experiment, $V_2(PO_4)_3$ could be obtained successfully as shown in Figure. 15a

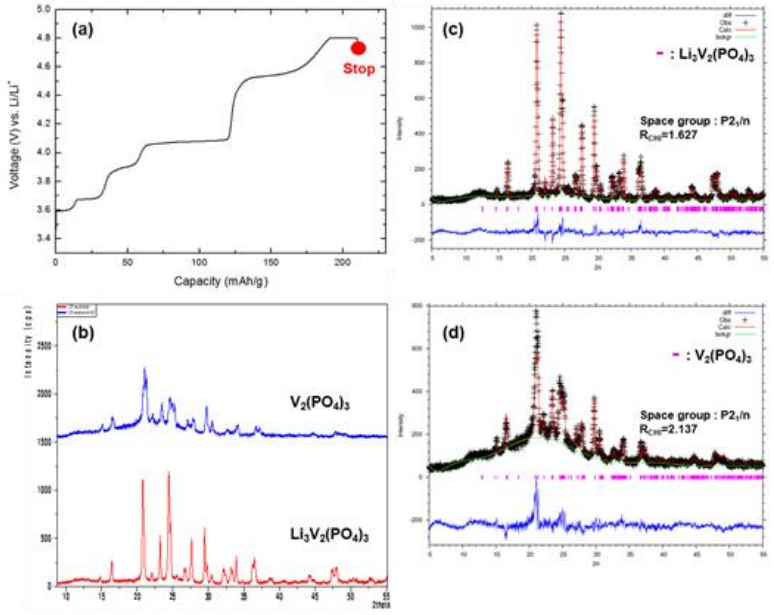

Fig. 15 (a) Galvanostatic delithiation voltage profile from $Li_3V_2(PO_4)_3$ to $V_2(PO_4)_3$ (b) XRD patterns of $Li_3V_2(PO_4)_3$ and $V_2(PO_4)_3$ electrode (c) XRD refinement of $Li_3V_2(PO_4)_3$ electrode by GSAS software (d) XRD refinement of $V_2(PO_4)_3$ electrode by GSAS software

The charge/discharge curve in Figure. 15a shows lithium ion extraction in the range of voltage. It is several step while lithium ion extracted. In general, $Li_3V_2(PO_4)_3$ was transferred three Li atoms when reversible electrochemical occurred (high theoretical capacity = 197mAh/g) [17]. Owing to operate at high voltage range of ~4.8V, cycle performance was quite poor. Next, through a XRD refinement of $V_2(PO_4)_3$ in Figure. 15d, it make confidently a decision that $V_2(PO_4)_3$ was prepared properly.

XRD patterns are refined same tool as $NaV_2(PO_4)_3$ using Rietveld analysis by GSAS program as shown in Fig. 15c and Fig. 15d. Refinement information of $Li_3V_2(PO_4)_3$ and $V_2(PO_4)_3$ made up lists with each atomic position and bonding distance in Table. 6 and Table. 7 ($Li_3V_2(PO_4)_3$) and Table. 8 and Table. 9 ($V_2(PO_4)_3$) as well as R factor are 1.627% and 2.137%. Moreover, we demonstrate how change the cell parameters of each material while lithium ion extracted. The unit cell volume shrunk about ~5.5% as shown in Table. 10.

Figure.15d illustrates $V_2(PO_4)_3$ electrode was fabricated as a pristine phase, therefore magnesium intercalation tests were carried out obtained electrode. Like a $Na_3V_2(PO_4)_3$, extraction process of $Li_3V_2(PO_4)_3$ by electrochemical test is, however, affected surface of electrode while cell assembled/disassembled.

Figure. 16 demonstrates the additional galvanostatic delithiation voltage profiles in the different voltage range (up to 4.2V). The reason why conducted these experiments is to compared with $NaV_2(PO_4)_3$ profiles.

Table 6. Crystallographic data of the Li3V2(PO4)3 electrode at room temperature

Atom	Type	Wyckoff	x	y	z	Occupancy	UISO
Li1	Li	4	0.2020	0.7810	0.1820	1	0.0125
Li2	Li	4	0.9340	0.3120	0.2260	1	0.0125
Li3	Li	4	0.5760	0.4290	0.2070	1	0.0125
V1	V	4	0.2510	0.4594	0.1094	1	0.0125
V2	V	4	0.7531	0.4745	0.3904	1	0.0125
P1	P	4	0.1069	0.0996	0.1586	1	0.0125
P2	P	4	0.6078	0.1149	0.3552	1	0.0125
P3	P	4	0.0395	0.2509	0.4885	1	0.0125
O1	O	4	0.9276	0.1163	0.1463	1	0.0125
O2	O	4	0.1482	0.9769	0.2404	1	0.0125
O3	O	4	0.1727	0.0516	0.0346	1	0.0125
O4	O	4	0.1618	0.2609	0.1845	1	0.0125
O5	O	4	0.4229	0.0912	0.3267	1	0.0125
O6	O	4	0.6959	0.0045	0.2841	1	0.0125
O7	O	4	0.6416	0.0876	0.4772	1	0.0125
O8	O	4	0.6437	0.2933	0.3143	1	0.0125
O9	O	4	0.9509	0.1284	0.5695	1	0.0125
O10	O	4	0.9307	0.3194	0.4028	1	0.0125
O11	O	4	0.1725	0.1630	0.4314	1	0.0125
O12	O	4	0.1059	0.3662	0.5761	1	0.0125

Table 7. Selected bond lengths (Å) of $Li_3V_2(PO_4)_3$ electrode

V1-O2	2.00336(20)	P3-Li1	3.05372(29)	O10-Li2	2.12947(23)
V1-O4	2.08082(15)	P3-Li3	3.06395(26)	O11-V1	1.93456(16)
V1-O5	2.03512(16)	O1-V2	2.02105(16)	O11-P3	1.53950(12)
V1-O7	1.88418(18)	O1-P1	1.55590(17)	O11-Li1	2.02205(15)
V1-O9	1.94337(18)	O1-Li2	1.93639(15)	O12-V2	1.87089(14)
V1-O11	1.93456(16)	O1-Li3	2.38952(18)	O12-V3	1.55166(11)
V1-Li1	2.93054(26)	O2-V1	2.00336(20)	Li1-V1	2.93054(26)
V1-Li1	2.96607(25)	O2-P1	1.48328(11)	Li1-V1	2.96607(25)
V1-Li3	3.03478(32)	O2-Li1	1.88375(15)	Li1-P1	2.87031(26)
V2-O1	2.02105(16)	O2-Li3	2.07875(21)	Li1-P1	2.95849(22)
V2-O3	1.88866(19)	O3-V2	1.88866(19)	Li1-P2	3.05402(27)
V2-O6	2.16537(23)	O3-P1	1.65407(16)	Li1-P3	3.05372(29)
V2-O8	2.03268(14)	O4-V1	2.08082(15)	Li1-O2	1.88375(15)
V2-O10	2.03290(16)	O4-P1	1.49611(13)	Li1-O4	1.98703(19)
V2-O12	1.87089(14)	O4-Li1	1.98703(19)	Li1-O5	1.95563(15)
V2-Li2	2.89033(22)	O4-Li2	2.07579(22)	Li1-O11	2.02205(15)
V2-Li3	2.69815(26)	O5-V1	2.03512(16)	Li1-Li2	3.32376(35)
P1-O1	1.55590(17)	O5-P2	1.63773(18)	Li1-Li3	3.03253(26)
P1-O2	1.48328(11)	O5-Li1	1.95563(15)	Li2-V2	2.89033(22)
P1-O3	1.65407(16)	O5-Li2	2.77329(22)	Li2-P1	2.49586(18)
P1-O4	1.49611(13)	O6-V2	2.16537(23)	Li2-P2	2.80194(24)
P1-Li1	2.87031(26)	O6-P2	1.49023(10)	Li2-O1	1.93639(15)
P1-Li1	2.95849(22)	O6-Li2	1.99962(15)	Li2-O4	2.07579(22)
P1-Li2	2.49586(18)	O6-Li3	2.06995(21)	Li2-O5	2.77329(22)
P1-Li3	2.70137(20)	O7-V1	1.88418(18)	Li2-O6	1.99962(15)
P2-O5	1.63773(18)	O7-P2	1.51238(16)	Li2-O8	2.73068(28)
P2-O6	1.49023(10)	O8-V2	2.03268(14)	Li2-O10	2.12947(23)
P2-O7	1.51238(16)	O8-P2	1.64030(14)	Li2-Li1	3.32376(35)
P2-O8	1.64030(14)	O8-Li2	2.73068(28)	Li2-Li3	3.24787(33)
P2-Li1	3.05402(27)	O8-Li3	1.83078(13)	Li2-Li3	3.38947(32)
P2-Li2	2.80194(24)	O9-V1	1.94337(18)	Li3-V1	3.03478(32)
P3-O9	1.62956(11)	O9-P3	1.62956(11)	Li3-V2	2.69815(26)
P3-O10	1.50602(13)	O9-Li3	2.02629(19)	Li3-P1	2.70137(20)
P3-O11	1.53950(12)	O10-V2	2.03290(16)	Li3-P3	3.06395(26)
P3-O12	1.55166(11)	O10-P3	1.50602(13)	Li3-O1	2.38952(18)
Li3-O2	2.07875(21)	Li3-O8	1.83078(13)	Li3-Li2	3.38947(32)
Li3-O6	2.06995(21)	Li3-O9	2.02629(19)		
Li3-Li1	3.03253(26)	Li3-Li2	3.24787(33)		

Table 8. Crystallographic data of the $V_2(PO_4)_3$ electrode at room temperature

Atom	Type	Wyckoff	x	y	z	Occupancy	UISO
V1	V	4	0.2470	0.4573	0.1239	1	0.0125
V2	V	4	0.7510	0.4794	0.3797	1	0.0125
P1	P	4	0.1000	0.1219	0.1483	1	0.0125
P2	P	4	0.6004	0.1199	0.3591	1	0.0125
P3	P	4	0.0348	0.2660	0.5087	1	0.0125
O1	O	4	0.9186	0.0950	0.1694	1	0.0125
O2	O	4	0.2087	0.0270	0.2350	1	0.0125
O3	O	4	0.1542	0.0799	0.0233	1	0.0125
O4	O	4	0.1268	0.2913	0.1788	1	0.0125
O5	O	4	0.4382	0.1084	0.3985	1	0.0125
O6	O	4	0.6427	0.0145	0.2705	1	0.0125
O7	O	4	0.7135	0.0778	0.4730	1	0.0125
O8	O	4	0.6571	0.2809	0.3182	1	0.0125
O9	O	4	0.9332	0.1817	0.6011	1	0.0125
O10	O	4	0.9253	0.3556	0.4336	1	0.0125
O11	O	4	0.0885	0.1287	0.4093	1	0.0125
O12	O	4	0.1677	0.3454	0.5564	1	0.0125

Table 9. Selected bond lengths (Å) of $V_2(PO_4)_3$ electrode

V1-O2	1.7998(5)	P2-O5	1.4401(5)	O5-V1	2.0442(6)
V1-O4	1.8499(4)	P2-O6	1.41317(34)	O5-P2	1.4401(5)
V1-O5	2.0442(6)	P2-O7	1.6900(5)	O6-V2	1.9830(6)
V1-O7	1.8170(6)	P2-O8	1.5274(4)	O6-P2	1.41317(34)
V1-O9	1.9822(6)	P3-O9	1.5459(4)	O7-V1	1.8170(6)
V1-O11	2.0474(5)	P3-O10	1.4948(4)	O7-P2	1.6900(5)
V2-O1	1.8371(5)	P3-O11	1.7059(4)	O8-V2	2.0062(5)
V2-O3	1.9237(6)	P3-O12	1.4305(4)	O8-P2	1.5274(4)
V2-O6	1.9830(6)	O1-V2	1.8371(5)	O9-V1	1.9822(6)
V2-O8	2.0062(5)	O1-P1	1.5629(6)	O9-P3	1.5459(4)
V2-O10	1.9238(5)	O2-V1	1.7998(5)	O10-V2	1.9238(5)
V2-O12	1.8098(5)	O2-P1	1.5981(4)	O10-P3	1.4948(4)
P1-O1	1.5629(6)	O3-V2	1.9237(6)	O11-V1	2.0474(5)
P1-O2	1.5981(4)	O3-P1	1.5668(5)	O11-P3	1.7059(4)
P1-O3	1.5668(5)	O4-V1	1.8499(4)	O12-V2	1.8098(5)
P1-O4	1.5050(5)	O4-P1	1.5050(5)	O12-P3	1.4305(4)

Table 10. The comparison of crystallographic data of the $Li_3V_2(PO_4)_3$ and $V_2(PO_4)_3$ electrode at room temperature

Materials	a (Å)	b (Å)	c (Å)	α	β	γ	Volume (Å^3)
$Li_3V_2(PO_4)_3$	8.6096	8.5922	12.0364	90.0000	90.5867	90.0000	890.40
$V_2(PO_4)_3$	8.4353	8.5220	11.7012	90.0000	89.0801	90.0000	841.15

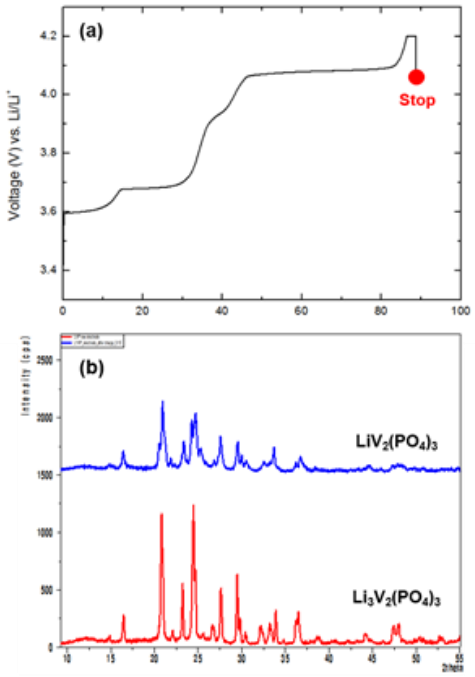

Fig. 16 (a) Delithiation process from $Li_3V_2(PO_4)_3$ to $LiV_2(PO_4)_3$ up to 4.2V (vs. Li/Li^+) by electrochemical extraction and (b) XRD patterns of $Li_3V_2(PO_4)_3$ and $LiV_2(PO_4)_3$

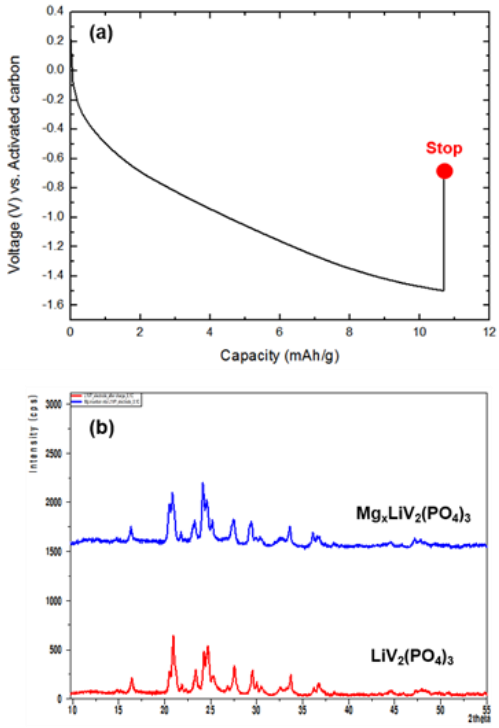

Fig. 17 (a) Magnesium insertion test into $LiV_2(PO_4)_3$ (b) XRD patterns of $LiV_2(PO_4)_3$ and $Mg_xLiV_2(PO_4)_3$

Figure. 17 shows the electrochemical Mg insertion process at 0.1C rate into $LiV_2(PO_4)_3$ with 0.5M $Mg(ClO_4)_2$ in acetonitrile electrolyte. Mg ion is difficult to intercalation into $LiV_2(PO_4)_3$ according to discharge curve in Figure. 17a. Discharge capacity is ~10mAh/g that seems to indeed difficulty as Mg ion intercalation into the host material. Figure 17b also gives an intimation in terms of unchanged XRD patterns.

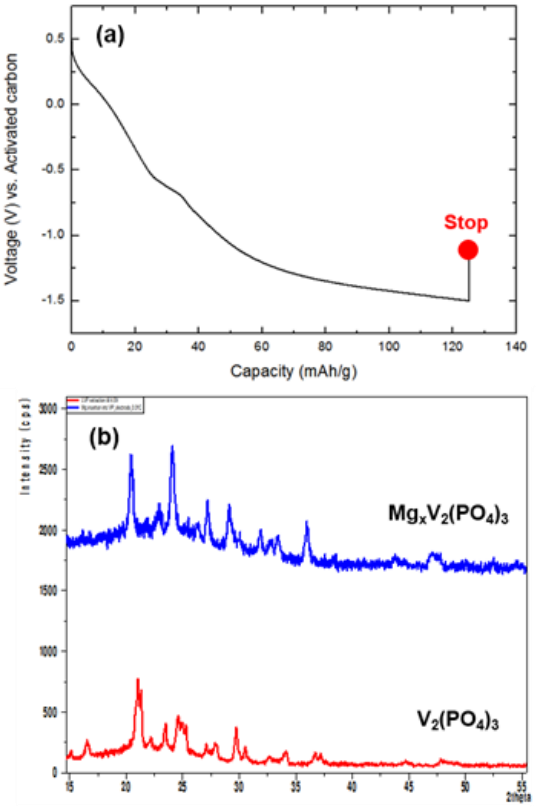

Fig. 18 (a) Magnesium insertion test into $V_2(PO_4)_3$ (b) XRD patterns of $V_2(PO_4)_3$ and $Mg_xV_2(PO_4)_3$

In contrast with $LiV_2(PO_4)_3$, $V_2(PO_4)_3$ shows the different behaviors with respect to discharge curve at 0.02C rate (Figure. 18a) and the change of XRD patterns (Figure. 18b). Discharge capacity is about ~120mAh/g in the voltage range of -1.5V vs. activated carbon. The voltage range of assumed Mg ion insertion is quite low by comparison of Mg metal (voltage vs. ~1.5V), nevertheless, we have got possibility of Mg ion intercalation into $V_2(PO_4)_3$. Figure 18b illustrates that XRD patterns were changed while Mg ion inserted. Although operational voltage is pretty low for utilizing high voltage Mg ion cathode materials, it is a deep significance that new electrode material, mono-$V_2(PO_4)_3$, candidate for Mg ion intercalation was investigated early stage of Mg rechargeable batteries.

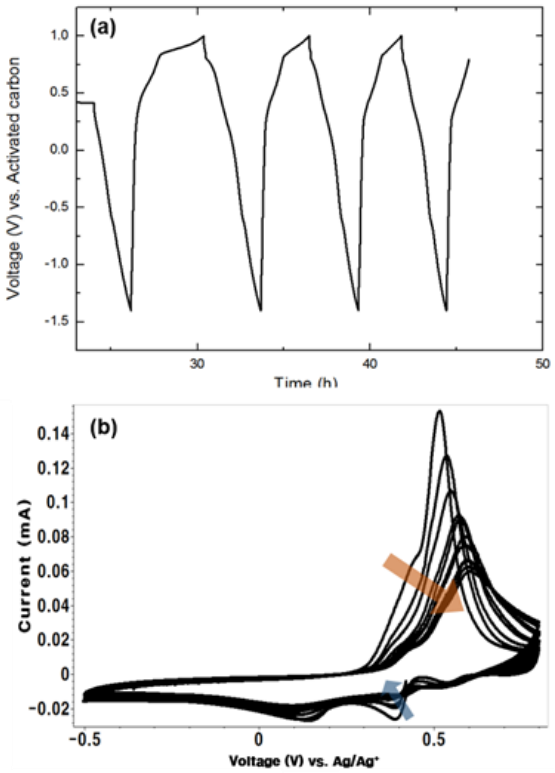

Fig. 19 Electrochemical Mg intercalation cycle test of (a) $V_2(PO_4)_3$ and (b) $LiV_2(PO_4)_3$

Figure. 19 shows the electrochemical profiles of $V_2(PO_4)_3$ and $LiV_2(PO_4)_3$.with 0.5M $Mg(ClO_4)_2$ in acetonitrile. In analyzing with Figure. 18a and Figure. 19a, the strong evidence have caught for Mg ion diffusion. The difference between two kinds of voltage profiles is a C-rate signal. Figure. 18a is 0.02C and Figure 19a is 0.1C. Depending on C rate conditions, first discharge profile has influenced as shown between fig. 18a and fig.19a. Relatively fast C rate, 0.1C, would be hindered in Mg intercalation on electrode/electrolyte interface. On the other hands, relatively slow C rate, 0.02C, carried out interface reaction smoothly than fast C rate. Next, we have investigated other two kinds of electrochemical profiles, Figure. 12 and Figure. 19b. The both data of CV profiles have similar patterns while cycle test was progressed. The two data have something in common. Above all, both materials have the other carrier ion into host materials causing to disturbance of Mg ion diffusion and by existing of two species atoms in the cell, it is difficult to determine the intercalated carrier ion when cell operation were conducted well. To prevent this confusion, this respect has considered when we have chosen new electrode materials

Conclusions

In summary, we investigated how magnesium ion intercalation reaction were occurred into the $NaV_2(PO_4)_3$ and $V_2(PO_4)_3$. Above all, those materials were prepared in submicron sized powder, and fabricated to electrodes. Its properties such as structural change, electrochemical performances were conducted. The following conclusions are classified by two parts of each material:

Ⅰ. $NaV_2(PO_4)_3$ - Structural change analysis have verified while sodium ions were extracted. Electrochemical reactions were occurred with 0.5M $Mg(ClO_4)_2$ in acetonitrile, nevertheless, its reactions could be determine whether magnesium ions were diffused or not because of the other carrier ion, sodium. In addition, surface of electrode has damaged due to several pre-experiment before implementing Mg intercalation experiment. In order to catch confident evidences with respect to magnesium ion intercalation, more elaborative technique with structural analysis and electrochemical experiments have to be carried out.

Ⅱ. $V_2(PO_4)_3$ - $V_2(PO_4)_3$ was also implemented like $NaV_2(PO_4)_3$ that structural analysis while sodium ions were extracted, and same electrochemical experiments using 0.5M $Mg(ClO_4)_2$ in acetonitrile electrolyte. In comparison with $NaV_2(PO_4)_3$, $V_2(PO_4)_3$ has no metal carrier ion such as Na ion. Mg ion intercalation into $V_2(PO_4)_3$ have confirmed by structural change and electrochemical test, even though capacity and cyclic performance were poor. This is because surface of $V_2(PO_4)_3$ electrode had also damaged due to electrochemical extraction step. Modifying synthesis process, the performance of mono-$V_2(PO_4)_3$ as a cathode material could be increased. Sad to say, we could not develop magnesium rechargeable battery using $NaV_2(PO_4)_3$ and $V_2(PO_4)_3$.

Although there are several matters to operate Mg rechargeable battery, several possibilities among those materials were discovered to improve profiles of Mg ion intercalation. Monoclinic-$V_2(PO_4)_3$ have attracted due to structural change and electrochemical properties during magnesium intercalations in this paper. Some solutions for magnesium ion intercalation were demanded, however, to increase kinetic properties of materials. Above all, particle size is a significant factor to determine Mg ion kinetic into host material, and coating process on particles surface using carbon or conducting material could be raised the kinetic performance of the material. The next thing is to design conditions of the chemical extraction process. In this study, we have discovered that the evidences that NASICON and NASICON-like structure could be developed as cathode materials for magnesium rechargeable batteries.

References

[1] Aurbach, D., et al. "Prototype systems for rechargeable magnesium batteries." Nature 407.6805 (2000): 724-727.

[2] Yoo, Hyun Deog, et al. "Mg rechargeable batteries: an on-going challenge." Energy & Environ-mental Science 6.8 (2013): 2265-2279.

[3] Prashant N. Kumta, et al. "Rechargeable magnesium battery: Current status and key challenges for the future." U.S. Progress in Materials Science 66 (2014): 1-86

[4] Muldoon, John, et al. "Electrolyte roadblocks to a magnesium rechargeable battery." Energy & Environmental Science 5.3 (2012): 5941-5950.

[5] Levi, Elena, et al. "$Cu_2Mo_6S_8$ Chevrel Phase, A Promising Cathode Material for New Rechargeable Mg Batteries: A Mechanically Induced Chemical Reaction." Chemistry of materials 14.6 (2002): 2767-2773.

[6] Saravanan, Kuppan, et al. "The first report on excellent cycling stability and superior rate capability of $Na_3V_2(PO_4)_3$ for sodium ion batteries." Advanced Energy Materials 3.4 (2013): 444-450.

[7] Yin, S-C., et al. "Electrochemical property: structure relationships in monoclinic $Li_{3-y}V_2(PO_4)_3$." Journal of the American Chemical Society 125.34 (2003): 10402-10411.

[8] Lin Gu, Xuekui, Zelang Jian, et al. "Atomic structure and kinetics of NASICON $Na_xV_2(PO_4)_3$ cathode for sodium ion batteries." Adv. Funct. Mater. 24, (2014): 4265-4272

[9] Zatovsky, Igor V. "NASICON-type $Na_3V_2(PO_4)_3$." Acta Crystallographica Section E: Structure Reports Online 66.2 (2010): i12-i12.

[10] H.S.Kim, T.S. Arthur, G.D. Allred, J. Zajicek, J.G. Newman, A.E. Rodnyansky, A.G. Oliver, W.C. Boggess, J. Muldoon, "Structure and compatibility of a magnesium electrolyte with a sulphur cathode", Nature Communications 2 (2011) 1

[11] E. Levi, MD Levi, O.Chasid, D.Aurbach "A review on the problems of the solid state ions diffusion in cathodes for rechargeable Mg batteries", Journal of the Electrochemical society 22 (2009) 13

[12] D.Imamura, M. Miyayama, M. Hibino, T. Kudo, "Mg Intercalation Properties into V2O5 gel/Carbon Composites under High-Rate Condition", Journal of the Electrochmeical Society 150 (2003) A753

[13] Z.L. Tao, L.N. Xu, X.L. Gou, J. Chen, H.T. Yuan, " TiS2 nanotubes as the cathode materials of Mg-ion batteries" Chemical Communications 18 (2004) 2080

[14] Y. Liang, R. Feng, S. Yang, H. Ma, J. Liang, J. Chen, "Rechargeable Mg Batteries with Graphene-like MoS2 Cathode and Ultrasmall Mg Nanoparticle Anode" Advanced Materials 23 (2010) 640

[15] A.Pan, JG.Zhang, Z.Nie, G.Cao, Bruce W. Arey, G.Li, S.Liang and J.Liu. " Facile synthesized nanorod structured vanadium pentoxide for high-rate lithium batteries "Journal of Materials Chemistry 20 (2010) 9193-9199

[16] Amir, N., et al. "Progress in nonaqueous magnesium electrochemistry." Journal of Power Sources 174.2 (2007): 1234-1240.

[17] Padhi, A. K., et al. "Mapping of transition metal redox energies in phosphates with NASICON structure by lithium intercalation." Journal of the Electrochemical Society 144.8 (1997): 2581-2586.